JEM Journal of Experimental Medicine

ARTICLE

IFITM3 incorporation sensitizes influenza A virus to antibody-mediated neutralization

Caroline Lanz[1,2*], Michael Schotsaert[3,4*], Carsten Magnus[1,5,6], Umut Karakus[1], Annika Hunziker[1,2], Milagros Sempere Borau[1,2], Carles Martínez-Romero[3,4], Eva E. Spieler[1,2], Sira C. Günther[1,2], Eva Moritz[1], Benjamin G. Hale[1], Alexandra Trkola[1], Adolfo García-Sastre[3,4,7,8], and Silke Stertz[1]

The disease severity of influenza is highly variable in humans, and one genetic determinant behind these differences is the *IFITM3* gene. As an effector of the interferon response, IFITM3 potently blocks cytosolic entry of influenza A virus (IAV). Here, we reveal a novel level of inhibition by IFITM3 in vivo: We show that incorporation of IFITM3 into IAV particles competes with incorporation of viral hemagglutinin (HA). Decreased virion HA levels did not reduce infectivity, suggesting that high HA density on IAV virions may be an antagonistic strategy used by the virus to prevent direct inhibition. However, we found that IFITM3-mediated reduction in HA content sensitizes IAV to antibody-mediated neutralization. Mathematical modeling predicted that this effect decreases and delays peak IAV titers, and we show that, indeed, IFITM3-mediated sensitization of IAV to antibody-mediated neutralization impacts infection outcome in an in vivo mouse model. Overall, our data describe a previously unappreciated interplay between the innate effector IFITM3 and the adaptive immune response.

Introduction

IFN-inducible transmembrane proteins (IFITMs) have been described as potent antiviral proteins that block the entry process of many different viruses, such as influenza A virus (IAV), HIV-1, Dengue virus, Zika virus, SARS-CoV-2, and others (Brass et al., 2009; Lu et al., 2011; Savidis et al., 2016; Shi et al., 2021). The antiviral potential of human IFITM1, IFITM2, and IFITM3 has been demonstrated ex vivo in tissue culture models for a diverse set of viruses, and also in vivo in the case of IAV. Human patients with a nonfunctional allele of IFITM3 or a mutation in the promoter region of IFITM3 have also been reported to possess an increased risk for severe IAV infections (Allen et al., 2017; Everitt et al., 2012). In line with this, *Ifitm3* knockout mice showed increased susceptibility to IAV and West Nile virus infection (Everitt et al., 2012; Gorman et al., 2016), highlighting the important role of IFITM3 in shaping viral pathogenicity.

The molecular mechanisms of IFITM-mediated viral inhibition are still under investigation. Current literature agree that cellular membranes show increased positive curvature and decreased membrane fluidity upon incorporation of IFITMs, offering a convincing explanation as to why IFITMs block fusion between cellular and viral membranes (Li et al., 2013; Lin et al., 2013; Rahman et al., 2020; Yount et al., 2012). In addition to their biophysical properties, IFITMs also rely on appropriate subcellular localization to exert their antiviral function. The presence of an N-terminal endocytosis motif in IFITM2 and -3 is responsible for endo-lysosomal targeting and is necessary for specifying antiviral activity against viruses that fuse in these compartments (Everitt et al., 2012; Jia et al., 2012; Jia et al., 2014; Spence et al., 2019; Suddala et al., 2019). Posttranslational palmitoylation of conserved cysteine residues is required for the clustering of IFITM3 in membranes, which, in turn, is a prerequisite for antiviral activity (McMichael et al., 2017; Yount et al., 2010).

While the inhibitory effect on viral entry exerted by IFITMs in target cells has been studied in detail, the consequences of IFITM activity in virus-producing cells is less well understood. Initially, it was observed that IFITM proteins become incorporated into budding HIV-1 virions and that this incorporation can be associated with a decrease in HIV-1 entry capacity (Compton et al., 2014; Tartour et al., 2014; Yu et al., 2015). In subsequent studies, it was demonstrated that this mode of action is not specific for HIV-1, but affects a diverse range of viruses,

[1]Institute of Medical Virology, University of Zurich, Zurich, Switzerland; [2]Life Sciences Zurich Graduate School, Eidgenössische Technische Hochschule Zurich and University of Zurich, Zurich, Switzerland; [3]Department of Microbiology, Icahn School of Medicine at Mount Sinai, New York, NY; [4]Global Health and Emerging Pathogens Institute, Icahn School of Medicine at Mount Sinai, New York, NY; [5]Department of Biosystems Science and Engineering, Eidgenössische Technische Hochschule Zurich, Basel, Switzerland; [6]Swiss Institute of Bioinformatics, Lausanne, Switzerland; [7]Department of Medicine, Icahn School of Medicine at Mount Sinai, New York, NY; [8]The Tisch Cancer Institute, Icahn School of Medicine at Mount Sinai, New York, NY.

*C. Lanz and M. Schotsaert contributed equally to this paper; Correspondence to Silke Stertz: stertz.silke@virology.uzh.ch.

including Ebola virus, measles virus, West Nile virus, and murine leukemia virus (MLV; Ahi et al., 2020; Tartour et al., 2017). The mode of virus assembly, as well as the type of viral glycoprotein, were found to impact virus sensitivity to this second antiviral function of IFITM3 (Appourchaux et al., 2019; Tartour et al., 2017; Yu et al., 2015). While the mechanism of inhibition is not resolved, it is assumed that IFITMs reduce the fusogenicity of virions, possibly by decreasing membrane fluidity. Moreover, a reduction in viral glycoprotein content by IFITMs has been suggested for HIV-1 and MLV, but, at least for HIV-1, these effects are discussed controversially (Ahi et al., 2020; Yu et al., 2015). Viruses thus need to be assessed individually for their susceptibility to IFITM-mediated inhibition in virus producer cells. A prominent example for which this information on IFITM action is missing is IAV.

Here, we investigated the incorporation of IFITM3 into IAVs and its impact on viral infectivity. We show that IFITM3 can be incorporated into IAV particles, which causes a reduction in the amounts of the viral glycoprotein hemagglutinin (HA) in virions. While artificial IAV virus-like particles (VLPs) with lower levels of glycoproteins displayed a decrease in infectivity, WT influenza viruses were found to be resistant to this mode of IFITM3-mediated viral inhibition. This suggests that high glycoprotein density is a viral strategy to evade this antiviral activity of IFITM3. Importantly, WT virus' sensitivity to antibody-mediated neutralization in vitro was increased upon incorporation of IFITM3. Mathematical modeling predicted that this leads to a substantial decrease and delay of peak viral titers in vivo. Verifying this prediction experimentally in an in vivo mouse model, we found that, indeed, protection by an HA-specific monoclonal antibody was diminished significantly in the absence of IFITM3. Thus, our data reveal a novel functional interplay between a host innate immune antiviral factor and the acquired antibody response, which is highly relevant for the outcome of influenza virus infection in vivo.

Results

IFITM3 present in producer cells restricts the entry capacity of pseudoviruses carrying IAV HA/neuraminidase (NA) or HIV-1 envelopes

We employed a pseudovirus (PV) system based on HIV-1 to address whether the presence of IFITM3 in producer cells leads to a reduction in the entry capacity of particles pseudotyped with IAV HA/NA (PV^{IAV}), similar to what has been described for viruses pseudotyped with HIV-1 Env (PV^{HIV}; Fig. 1 a; Compton et al., 2014; Tartour et al., 2014). We transfected HEK 293T cells with pNL-LucAM, a plasmid encoding the HIV-1 strain NL4-3 genome in which the envelope gene is replaced by a luciferase gene (Pugach et al., 2007), together with plasmids encoding the envelope genes from HIV-1 strain JRFL, IAV A/WSN/33 or vesicular stomatitis virus (VSV), or an empty vector plasmid as a no-envelope control, in the presence or absence of Flag-tagged IFITM3. PVs produced under these conditions were purified and analyzed for IFITM3 incorporation by Western blotting for the Flag epitope, as previous studies had shown that copurification of IFITM3 with HIV-1 particles correlates with virion incorporation of IFITM3 (Compton et al., 2014; Tartour et al., 2014; Tartour et al., 2017). All PVs exhibited a strong Flag signal, suggesting that IFITM3 was indeed incorporated and that incorporation occurred independently of any envelope (Fig. 1 b). Of note, the presence of IFITM3 did not impact the amount of p24 detected, suggesting that VLP release efficiency is not affected by IFITM3 (Fig. 1 b). PVs produced in the absence of IFITM3 were subsequently tested for their infectivity on A549 human lung epithelial cells or TZM-bl cells, which are HeLa cells engineered to express the HIV-1 receptors (CD4 and CCR5) and an LTR-driven luciferase reporter (Montefiori, 2005; Platt et al., 1998; Wei et al., 2002). While A549 cells could only be infected with PV^{IAV} and PV^{VSV} (Fig. S1 a), TZM-bl cells were susceptible to PV^{HIV} and PV^{VSV} (Fig. S1 b). Thus, A549 cells were selected to test the impact of incorporated IFITM3 on PV^{IAV}, whereas TZM-bl cells were suitable for PV^{HIV}. We then compared the infectivity of PVs produced in the presence or absence of IFITM3 by infecting cells with p24-normalized amounts of PV. PV^{IAV} and PV^{HIV} were restricted in their infectivity when produced in cells expressing IFITM3, while PV^{VSV} was not affected by the presence of IFITM3 in producer cells (Fig. 1, c and d). This effect was specific to IFITM3 expression, as overexpression of the epidermal growth factor receptor (EGFR) to represent a control membrane-localized protein did not result in inhibition of PV^{IAV} infection (Fig. 1 e). Thus, we conclude that incorporation of IFITM3 into PV particles possessing IAV envelopes leads to decreased infectivity, similar to what has been observed for HIV-1.

To compare the magnitude of inhibition of PV infectivity by IFITM3 presence in producer cells with the previously described inhibition of infection by IFITM3 in target cells (Brass et al., 2009; Feeley et al., 2011), we generated A549 and TZM-bl cells stably expressing IFITM3. We then infected A549 cell lines with PV produced in the presence or absence of IFITM3 and observed a significant reduction in PV^{IAV} entry in A549-IFITM3 cells (Fig. S1, c and d). Intriguingly, a comparable decrease in infectivity was observed when IFITM3 was present in producer cells only (Fig. S1 d). Likewise, PV^{HIV} infection was influenced by IFITM3 presence in both producer and target TZM-bl cells (Fig. S1 e). PV^{VSV} was significantly inhibited in infectivity when IFITM3 was expressed in target cells, but the presence of IFITM3 in producer cells led to no reduction in infectivity (Fig. S1 f). Thus, in the HIV-based PV system, incorporation of IFITM3 into particles carrying an IAV envelope has similar antiviral potency compared with the known entry inhibition of IAV by IFITM3 in target cells.

IFITM3 in producer cells inhibits the entry capacity of IAV-VLPs by outcompeting HA incorporation

To verify our findings, we employed an IAV-based VLP system (Fig. 2 a) in which plasmids encoding a β-lactamase–M1 (BlaM1) fusion protein, IAV HA, NA, and M2—in the presence or absence of IFITM3—are transfected into HEK 293T cells to generate IAV-VLPs (Tscherne et al., 2010). The entry efficiency of these VLPs can be assessed by loading target cells with CCF2, a fluorogenic substrate that shifts in emission upon cleavage by the β-lactamase carried into the cell by the infecting VLP. This assay directly measures entry without relying on transcription or other downstream events, as in the HIV-1–based PV system. IAV-VLPs produced in the absence or presence of IFITM3 were

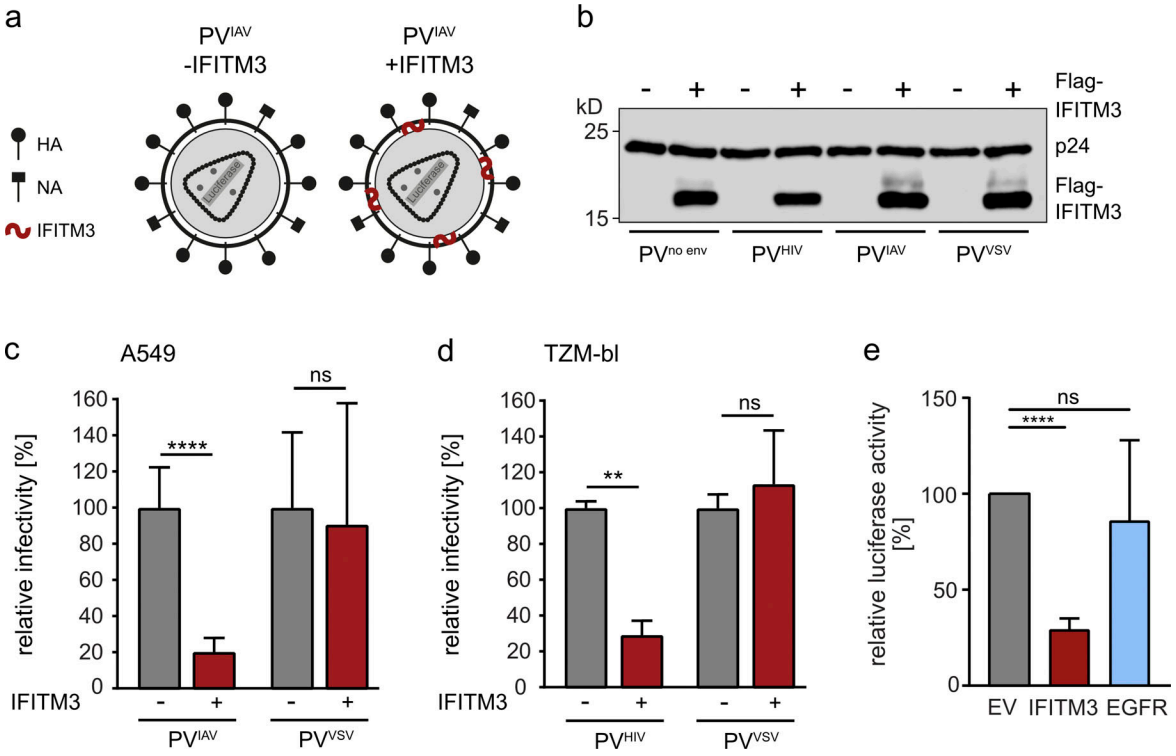

Figure 1. **IFITM3 present in producer cells restricts the entry capacity of PVs carrying IAV and HIV-1 envelopes. (a)** Schematic depiction of the HIV-1–based PVs carrying IAV envelopes (PV^{IAV}) produced in the absence or presence of IFITM3. **(b)** PVs were purified and concentrated by ultracentrifugation through a 20% sucrose cushion, normalized via p24 ELISA, and analyzed by Western blot. Membrane was stained with anti-Flag and anti-p24 antibodies. **(c and d)** A549 cells (c) or TZM-bl cells (d) were infected for 48 h with the indicated PVs produced in the absence or presence of IFITM3. Luciferase was measured and infectivity was calculated by setting values obtained from PVs produced in the absence of IFITM3 to 100%. **(e)** A549 cells were infected for 48 h with the indicated PVs produced in the absence or presence of IFITM3 or EGFR. Luciferase was measured and infectivity was calculated by setting values obtained from PVs produced in the presence of the vector control (EV) to 100%. **(c–e)** Mean values from three biological replicates, each performed in triplicates, are shown. Error bars represent SD. Statistical significance was assessed by a paired two-tailed Student's *t* test. **, P < 0.01; ****, P < 0.0001.

purified and subjected to Western blot analysis. A distinct Flag-IFITM3 band was detected in IAV-VLPs produced in IFITM3-expressing cells, suggesting that, similar to PV^{IAV}, IFITM3 also incorporates into IAV-VLPs (Fig. 2 b). Strikingly, we observed a 26% decrease in HA protein incorporation into IAV-VLPs produced in the presence of IFITM3 when we quantified HA levels and normalized to BlaM1 levels (Fig. 2 b). Furthermore, there was a trend toward a decrease in NA activity in IFITM3-containing VLPs, suggesting also a reduced incorporation of NA (Fig. 2 c). This decrease in glycoprotein content was also evident in IAV PVs (PV^{IAV}), where we observed a 55% reduction in HA incorporation—normalized to p24 levels—when PVs were produced in the presence of IFITM3, but not another membrane-localized protein (Fig. S2, a–d). Of note, the levels of VSV-G in PV^{VSV} were not reduced by IFITM3 expression but the levels of envelope in PV^{HIV} seemed to be reduced, even though this did not reach statistical significance, suggesting that IFITM3-mediated reductions in glycoprotein levels in the virion correlate with a decrease in infectivity. Importantly, total levels of HA in producer cells were largely unaffected by IFITM3 expression (Fig. S3 a). When probing the IAV-VLPs for infectivity in MDCKII cells, we observed a 60% reduction in entry efficiency for VLPs produced in the presence of IFITM3 (Fig. 2 d). In contrast to the PV^{IAV} system, this reduction in entry efficiency was lower for IFITM3 expressed in producer cells compared with IFITM3 expression in target cells (Fig. S3 b). From these results, we hypothesized that IFITM3 may compete with the viral glycoproteins for incorporation into viral particles. As localization to the same plasma membrane areas would be a prerequisite for competition, we analyzed the distribution of IFITM3 and HA in transfected A549 and HEK 293T cells by immunofluorescence (IF) staining. While a large fraction of IFITM3 displayed the expected endosomal distribution, as previously reported, we also observed accumulation of IFITM3 and HA in the same patches of the plasma membrane, suggesting that competition for incorporation could occur (Fig. 2 e; Compton et al., 2016; Tartour et al., 2014). Next, we tested whether IAV HA or NA would outcompete the negative effect of IFITM3 on IAV-VLP infectivity when present in producer cells. IAV-VLPs were produced in HEK 293T cells transfected with a constant amount of IFITM3—or the empty vector as a negative control—in the presence of increasing amounts of HA or NA. Western blot analysis of these IAV-VLPs confirmed that transfecting increasing amounts of HA led to increased amounts of HA present in IAV-VLPs (Fig. 2 f). Furthermore, we confirmed our previous observation that IFITM3 reduced the amount of HA incorporated into IAV-VLPs. Interestingly, in

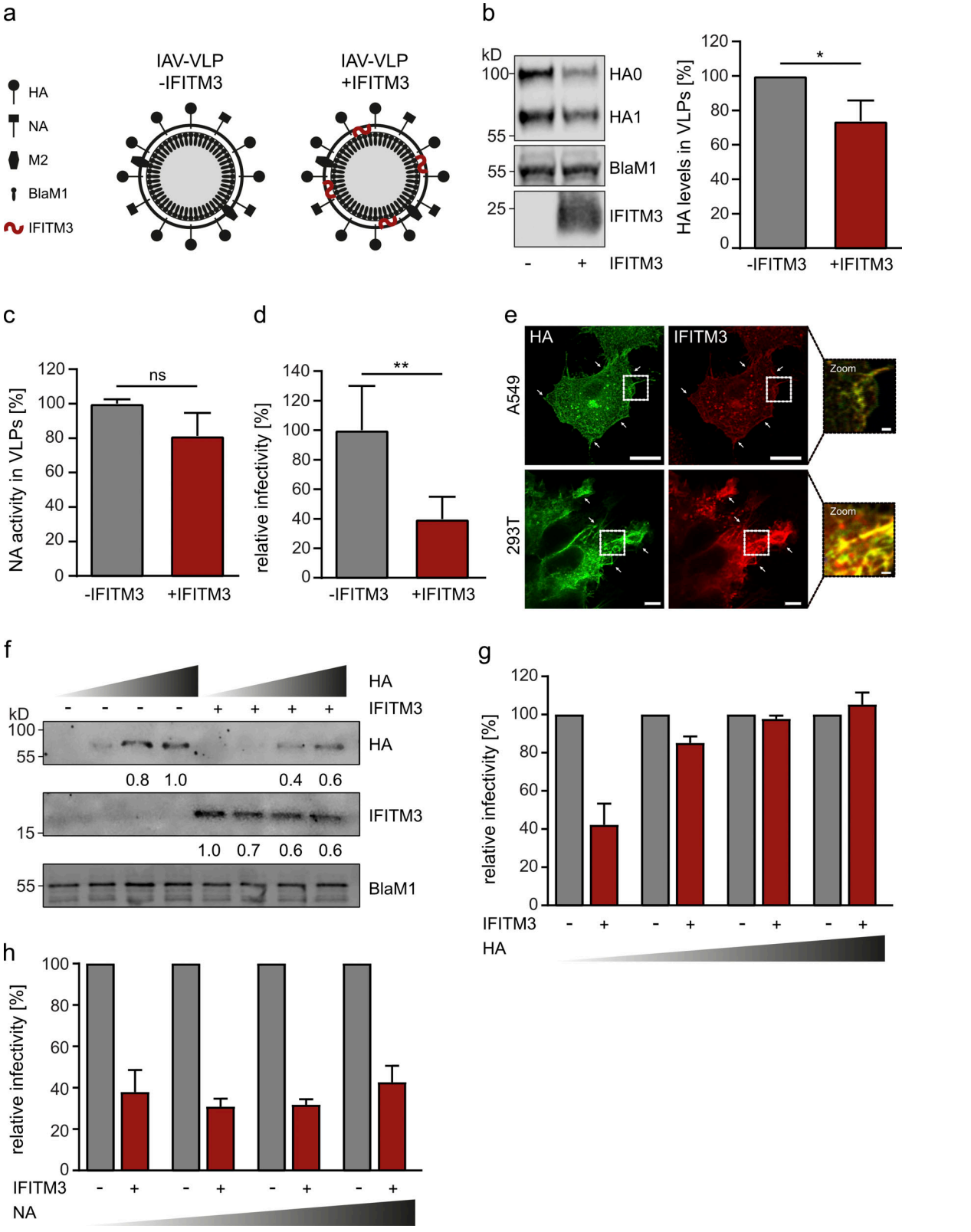

Figure 2. **IFITM3 in VLP-producing cells restricts the entry capacity of IAV-VLPs by outcompeting HA incorporation. (a)** Schematic depiction of IAV-VLPs produced in the absence or presence of IFITM3. **(b)** VLPs were purified by ultracentrifugation and analyzed by Western blot using a polyclonal antibody against A/WSN/33 and an antibody against IFITM3. A representative blot is shown on the left, and the quantification of HA band intensities normalized to BlaM1 levels from three independent batches of VLPs is shown on the right. Statistical significance was assessed by an unpaired two-tailed Student's *t* test. *, $P < 0.05$. **(c)** The NA content of VLPs was determined using the NA-Star Influenza Neuraminidase Inhibitor Resistance Detection Kit. Bars represent the mean of three biological replicates with the error bars representing SD. Statistical significance was assessed by an unpaired two-tailed Student's *t* test. **(d)** IAV-VLPs

produced in the presence or absence of IFITM3 were normalized via Western blot for equal M1 levels and used to infect MDCKII cells. VLP entry-positive cells were assessed by flow cytometry, and infectivity was normalized to the values obtained for VLPs produced in the absence of IFITM3. Bars represent the mean of three biological replicates, with the error bars representing SD. Statistical significance was assessed by a paired two-tailed Student's *t* test. **, P < 0.01. **(e)** A549 (top) or 293T cells (bottom) were transfected with HA- and IFITM3-expressing constructs for 24 h, and then fixed and stained for HA (green) and IFITM3 (red). Samples were analyzed by confocal microscopy. Representative cells are shown with areas of colocalization highlighted at higher magnification. Scale bars correspond to 15 µm (A549), 5 µm (293T), or 1 µm (both zoom images). **(f)** IAV-VLPs with increasing amounts of HA were produced in the presence or absence of IFITM3 and analyzed by Western blot. Membrane was stained using a polyclonal antibody against A/WSN/33 proteins and a Flag antibody. HA and Flag-IFITM3 band intensities were determined and normalized to BlaM1. A quantification of the levels of HA and IFITM3 in relation to the strongest band are given below the respective Western blots. **(g)** IAV-VLPs containing increasing amounts of HA were produced in the absence or presence of IFITM3 and were used to infect MDCKII cells. For each condition, infectivity of VLPs produced in the absence of IFITM3 was set to 100%. Bars represent the mean of three biological replicates with the error bars representing SD. **(h)** IAV-VLPs containing increasing amounts of NA were produced in the absence or presence of IFITM3 and were used to infect MDCKII cells. For each condition, infectivity of VLPs produced in the absence of IFITM3 was set to 100%. Bars represent the mean of two biological replicates with the error bars representing SD.

the presence of IFITM3, the increase in HA incorporation was paralleled by a decrease in IFITM3 incorporation (Fig. 2 f). When we assessed the infectivity of these IAV-VLPs, we found that the negative effect of IFITM3 on IAV-VLP infectivity was alleviated in a dose-dependent manner by an increase in HA (Fig. 2 g). In contrast, increasing the amount of NA did not counteract the inhibitory effect of IFITM3 on IAV-VLP infectivity (Fig. 2 h). Of note, coexpression of IFITM1 also led to a decrease in IAV-VLP infectivity that could be overcome by higher levels of HA (Fig. S3 c).

IFITM3 incorporates into IAV particles, but does not directly impact infectivity

Our experiments so far showed that IFITM3 present in producer cells negatively affects the infectivity of PV^{IAV} and IAV-VLPs, and that this is dependent on the levels of HA incorporation. To address whether this was also true for authentic IAV, we infected naive A549 cells or IFITM3-expressing A549 cells with A/WSN/33 at a multiplicity of infection (MOI) of 0.01 PFU/cell for 48 h (naive A549 cells) or 72 h (A549-IFITM3 cells; Fig. 3 a). Importantly, the levels of ectopic IFITM3 were slightly lower than the levels of IFITM3 induced by IFN-α, and thus IFITM3 levels were in a physiological range (Fig. S4 a). The chosen infection conditions allowed the virus to grow to similar titers in naive and IFITM3-expressing cells. When purifying virus from supernatants and analyzing protein content by Western blot, we observed an IFITM3 band similar to that observed for PV^{IAV} and IAV-VLPs, suggesting that IFITM3 is incorporated into authentic IAV particles (Fig. 3 b). Consistent with our data obtained for PV^{IAV} and IAV-VLPs, HA levels were reduced by 27% in virus cultured on IFITM3-expressing cells compared with virus grown on control cells (Fig. 3 b). Furthermore, colocalization of HA and IFITM3 in patches at the plasma membrane was observed in IAV-infected A549-IFITM3 cells (Fig. S4 b), suggesting a plausible mechanism of competition for incorporation. To exclude that these observations were a strain-specific effect, we also grew the pandemic H1N1 strain A/Netherlands/602/2009 in the presence or absence of IFITM3. We measured a similar reduction (30%) in HA content for virions grown in the presence of IFITM3 (Fig. 3 c). To clarify whether IFITM3 indeed incorporates into IAV particles, we subjected our samples to immunostaining for IFITM3, followed by electron microscopy. While none of the particles produced in the absence of IFITM3 had any IFITM3-specific labeling (n = 13), 15 of 28 imaged virions grown in the presence of IFITM3 displayed IFITM3-specific labeling of the viral membrane (Fig. 3 d). Thus, we conclude that IFITM3 can be incorporated into authentic IAV particles and compete for HA incorporation.

To compare the infectivity of IFITM3-positive and -negative viruses, we performed a sensitive luciferase-based IAV minigenome reporter assay using quantitative RT-PCR (RT-qPCR)–normalized viral inputs. Strikingly, and in contrast to the results obtained with PV^{IAV} and IAV-VLPs, IAV grown on IFITM3-expressing cells was not impaired in its infectivity compared with IAV cultured on control cells (Fig. 3 e). To understand why this IFITM3-mediated loss of HA incorporation in authentic IAV particles did not result in a loss of infectivity, we analyzed producer cell lysates from IAV, PV^{IAV}, and IAV-VLP samples. The producer cell lysates of PV^{IAV} displayed a 76-fold-higher IFITM3:HA ratio than the lysates from the IAV-infected cells (Fig. 3 f). In accordance with our previous results, this higher ratio of IFITM3:HA led to a stronger reduction in HA content in the respective viral particle preparations (55% for PV^{IAV} [Fig. S2 b] versus 27% for IAV [Fig. 3 b]). The lysates of the producer cells for IAV-VLPs displayed a threefold-higher ratio of IFITM3:HA than the lysates of IAV infected cells (Fig. 3 f), but the reduction in HA content was similar (26% for IAV-VLPs [Fig. 2 b] versus 27% for IAV [Fig. 3 b]). Of note, the amounts of HA in relation to M1 levels were four- to sixfold higher in infected cells compared with IAV-VLP–producing cells (Fig. 3 f), suggesting that IAV particles display higher levels of HA relative to their M1 content than the IAV-VLPs, and that this may counteract the impact of IFITM3 incorporation on infectivity. Indeed, when we compared the HA:M1 ratio in three independent batches of purified IAV versus IAV-VLPs, we detected an approximately fourfold-higher HA content in IAV particles (Fig. 3 g). These data show that the relative amount of HA is substantially higher in IAV particles compared with IAV-VLPs, and this may render IAV relatively resistant to the direct inhibitory effect of IFITM3 incorporation.

IFITM3 increases the sensitivity of IAV to HA-directed antibody-mediated neutralization

While IAV infectivity was not directly impaired by the reduction of HA incorporation inflicted by IFITM3 expression, we hypothesized that, in vivo, reduced levels of HA may still affect IAV. A setting in which HA levels may play a substantial role is during neutralization by HA-targeting antibodies, where a reduction of HA on IAV virions by IFITM3 could potentially render

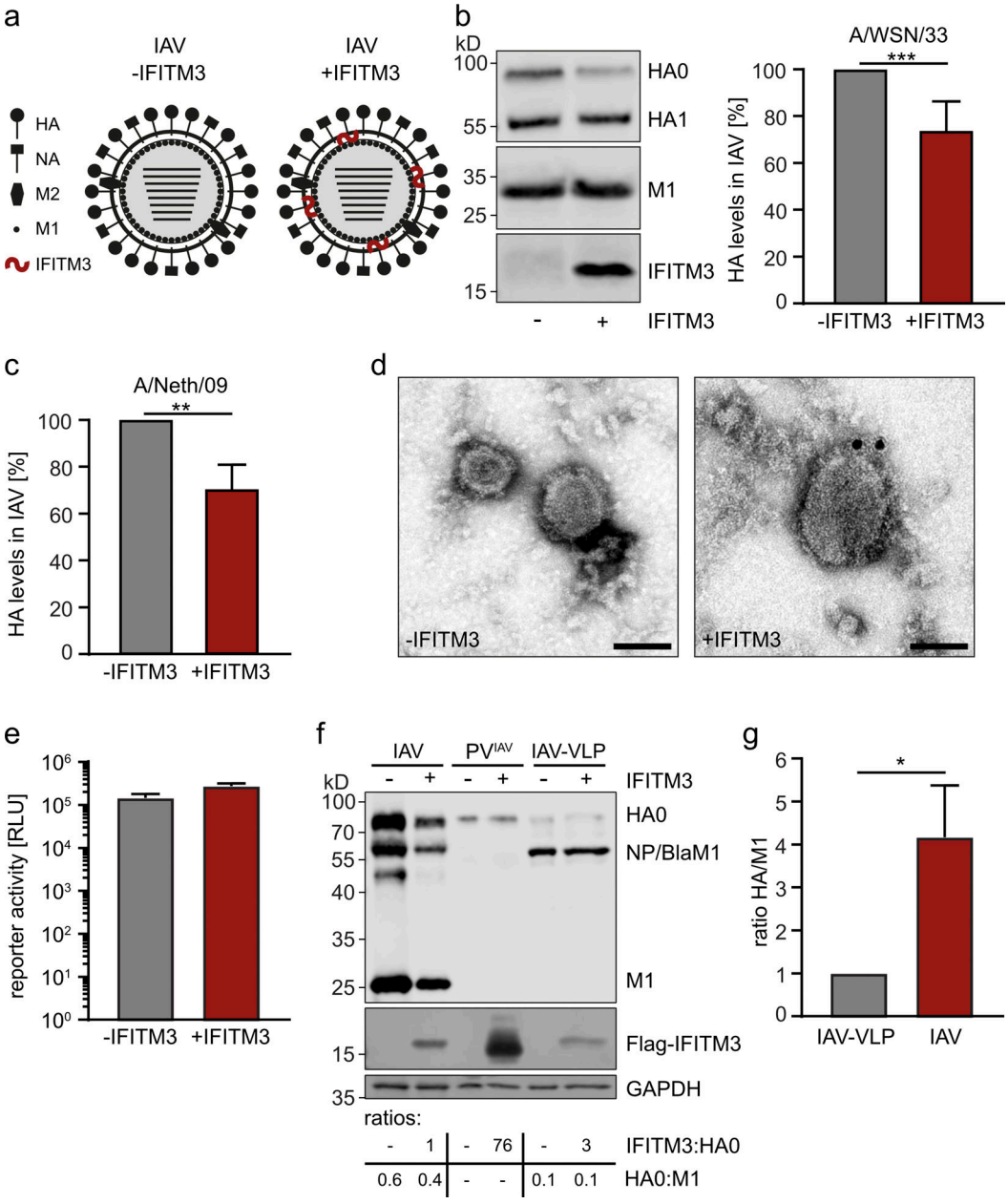

Figure 3. **IFITM3 incorporates into IAV particles, but its antiviral effect is antagonized by high HA density. (a)** Schematic depiction of IAV produced in the absence or presence of IFITM3. **(b)** A549 control or A549-IFITM3 cells were infected with IAV strain A/WSN/33 at MOI 0.01 PFU/cell for 48 h in case of the control cells or 72 h in case of the IFITM3-expressing cells. Viruses in the supernatants were purified by ultracentrifugation and analyzed by Western blot for HA, M1, and IFITM3. A representative blot is shown on the left, and the quantification of HA band intensities normalized to M1 levels from six independent batches of viruses is shown on the right. Statistical significance was assessed by an unpaired two-tailed Student's *t* test. ***, $P < 0.0005$. **(c)** IAV strain A/Netherlands/602/2009 (A/Neth/09) was grown on MDCK control or MDCK-IFITIM3 cells, purified by ultracentrifugation, and analyzed by Western blot for HA, M1, and IFITM3. HA band intensities from four independent sets of virus preparations were measured, normalized to M1 levels, and plotted relative to normalized HA levels for virus grown in the absence of IFITM3. Error bars represent SD, and statistical significance was assessed by an unpaired two-tailed Student's *t* test. **, $P < 0.005$. **(d)** The purified viruses described in panel b were analyzed by immuno-electron microscopy using a polyclonal anti-IFITM3 antibody. Scale bars correspond to 100 nm. **(e)** HEK 293T cells were transfected with a reporter plasmid encoding firefly luciferase in complementary reverse orientation flanked by IAV noncoding regions, thus mimicking a viral genome segment. Cells were subsequently infected with the viruses described in panel b, which were input normalized by RT-qPCR. Luciferase signal was measured as relative light units (RLUs) 48 h after infection. Bars represent the mean of three biological replicates with the error bars representing SD. **(f)** A549 control or A549-IFITM3 cells infected with A/WSN/33 (from panel b), PV^{IAV}-producing cells (from Fig. 1, b and c), and IAV-VLP producer cells (from Fig. 2, b–d) were lysed and analyzed by Western blot using a polyclonal antibody against A/WSN/33 proteins and antibodies against Flag and GAPDH. Relative Flag-IFITM3:HA0 and HA0:M1 ratios for each condition are given below the Western blot. **(g)** IAV-VLPs produced in the absence or presence of IFITM3 and viruses grown on A549 control or A549-IFITM3 cells were compared side by side in Western blots stained for HA and M1. The average ratios of HA levels normalized to M1 levels from three independent batches of VLPs or viruses are shown. Statistical significance was assessed by an unpaired two-tailed Student's *t* test. *, $P < 0.05$.

the virus more neutralization sensitive. First, we adapted a mathematical modeling approach for virus entry and neutralization (Brandenberg et al., 2017) to take into account known entry stoichiometry data for IAV. The number of HA trimers per influenza virion had initially been estimated by biochemical approaches to range from 340 to 400 trimers (Inglis et al., 1976). A cryo-electron microscopy study refined this range and determined that an average spherical influenza virus particle contains ∼300 trimers of HA (Harris et al., 2006). Furthermore, the number of HA trimers required for binding has been estimated to be between 20 to 30, while the number of trimers required for fusion has been determined to be three to four (Danieli et al., 1996; Floyd et al., 2008; Ivanovic et al., 2013). For neutralization, stoichiometry ratios of ≤1 were reported, indicating that only one of three HA subunits needs to be neutralized for the HA trimer to lose its functionality (Knossow et al., 2002; Otterstrom et al., 2014). Using these parameters, we established a model for IAV neutralization and applied this model to probe the impact of a reduction in the virions' HA content on antibody-mediated neutralization. Our model predicted that a reduction in HA trimer content by 27%, as observed upon IFITM3 incorporation into IAV (Fig. 3 b), would lead to an increase in neutralization sensitivity for antibodies that interfere with viral binding to the host cell (Fig. 4 a).

To test this prediction, the IAV strain A/WSN/33 grown on naive or IFITM3-expressing cells was normalized by RT-qPCR for the M segment and preincubated with a dilution series of a monoclonal anti-A/WSN/33 HA antibody, which possesses hemagglutination inhibition activity and therefore prevents virus binding, before being used to infect MDCKII cells. We observed an increase in neutralization sensitivity for the virus grown on IFITM3-expressing cells (Fig. 4 b). The same result was observed when we used a polyclonal rabbit serum raised against IAV A/WSN/33, which also inhibits virus binding (Fig. 4 c).

Next, we employed our mathematical model to predict the impact of IFITM3 incorporation on virus neutralization by antibodies targeting the HA-mediated membrane fusion step. For these antibodies, the model predicts a less pronounced difference in neutralization sensitivity between viruses with and without incorporated IFITM3 (Fig. 4 d). We performed a neutralization assay with two different broadly neutralizing HA-directed antibodies (mAb 1.12; mAb 3.1) that had previously been shown to target epitopes in the HA stem (Wyrzucki et al., 2015; Wyrzucki et al., 2014). Both antibodies do not display any hemagglutination inhibition activity, but potently neutralize IAV and thus presumably inhibit viral entry by blocking the fusion process (Wyrzucki et al., 2015). In line with the predictions from our model, IAV A/WSN/33 produced on IFITM3-expressing cells did not display an increase in neutralization sensitivity to either of the two stem-directed antibodies (Fig. 4, e and f). Next, we tested if the observed increase in neutralization sensitivity by IFITM3 was also detectable with human sera from IAV-vaccinated individuals. For this, we performed neutralization assays using the 2009 pandemic IAV isolate A/Netherlands/602/2009 grown in the absence or presence of IFITM3. Similar to the results for A/WSN/33, we observed an IFITM3-mediated increase in neutralization sensitivity of A/Netherlands/602/2009 to an HA head-targeting monoclonal antibody (Fig. 4 g), as well as two different human sera from individuals vaccinated against the pandemic virus (Fig. 4, h and i). We thus conclude that the incorporation of IFITM3 into authentic IAV particles increases the virus' sensitivity to HA-directed monoclonal antibodies and human vaccine sera that interfere with virus binding to target cells.

IFITM3-mediated enhanced sensitivity of IAV to antibody-based neutralization impacts viral growth and pathogenicity in vivo

To determine if IFITM3-mediated enhanced sensitivity to neutralization by antibodies plays a role in vivo, we first employed our modeling approach and found that a wide range of IFITM3-mediated reductions in HA trimer content would lead to an increase in neutralization sensitivity for antibodies that interfere with viral binding to the host cell (Fig. 5 a). Next, we aimed to compare the effect of neutralization on replicative fitness and virus dynamics of IAV grown in the presence or absence of IFITM3. The replicative fitness defines the number of infected cells that one infected cell produces in a fully susceptible population of host cells. For our model, we used a baseline reproductive fitness of F_0 = 10.8 for IAV, which was determined in previous work (Baccam et al., 2006). This means that, in the absence of neutralizing antibodies, one cell infected with IAV will infect, on average, 10.8 other cells. To determine replicative fitness as a function of antibody concentration, we implemented a mathematical model based on previous work on HIV-1 neutralization (Magnus et al., 2016). In this framework, antibody neutralization reduces replicative fitness. Our results suggest that IFITM3 incorporation leads to a decrease in viral fitness for antibodies that interfere with binding (Fig. 5 b). Of note, our model only considers IFITM3-mediated reduction of HA density, but not IFITM3-mediated entry inhibition in target cells, as we aimed to assess only the impact of our novel mode of virus inhibition. To examine whether these small reductions in viral fitness could impact virus dynamics in vivo, we extended a within-host virus dynamics model for IAV (Baccam et al., 2006; Domingues et al., 2019). This model describes the viral load over time of infection. First, we determined the antibody concentration at which the effect on viral dynamics is the highest for antibodies targeting the binding step ($c[Ab] = 1.05 \times 10^{-09}$). Using this concentration and the 27% reduction in HA content observed, we modeled virus dynamics in vivo and found that for antibodies acting on virus binding, a 10-fold reduction and a delay of 4 d for peak viral loads was predicted in the presence of IFITM3 (Fig. 5 c). This reduction and delay in virus replication should allow the immune system to better control the infection and thus result in reduced pathogenicity. When reductions in HA content of 40% or 60% were used as input, our model even predicted complete abrogation of viral replication in the presence of IFITM3 (Fig. 5 c). To enable additional testing of different parameter modifications, such as reduction in HA content or stoichiometry of virus binding, we developed an app (https://magnuscar.shinyapps.io/FluStoich/) where the impact of multiple parameters can be assessed and predictions can be visualized. Overall, our modeling results suggest that

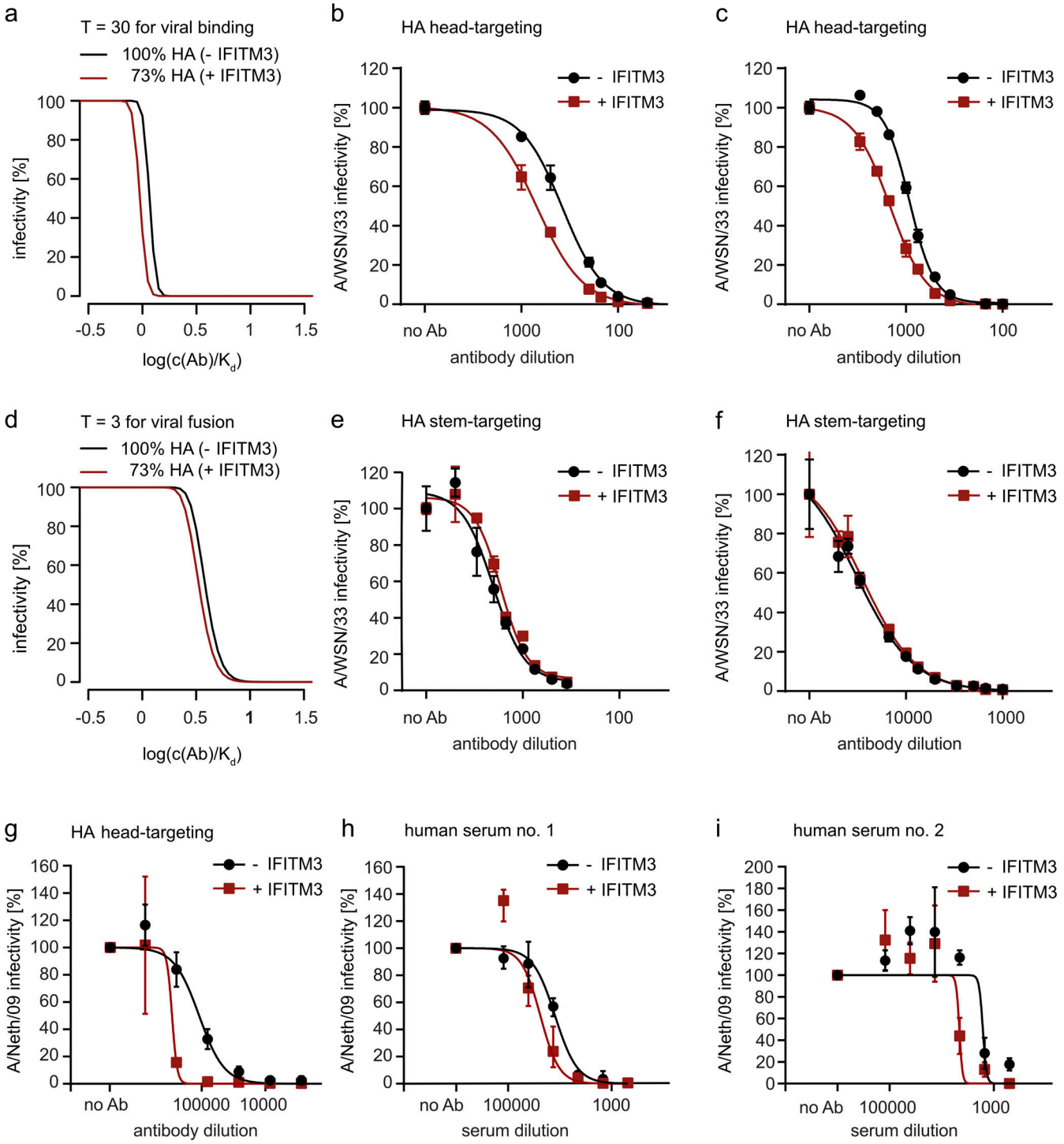

Figure 4. **Incorporation of IFITM3 into IAV increases sensitivity to antibody-mediated neutralization. (a)** Predicted inhibition curves of antibodies interfering with IAV binding to host cells for IAV with regular trimer number (300 trimers/virion, black line) and a trimer number reduced by 27% as observed upon IFITM3 incorporation (219 trimers/virion, red line). **(b and c)** IAV A/WSN/33 produced in A549 control or A549-IFITM3 cells was input normalized by RT-qPCR and incubated with different dilutions of a monoclonal anti-A/WSN/33 HA antibody (b) or a polyclonal rabbit serum raised against IAV strain A/WSN/33 (c) before being used to infect MDCK cells. Cells were fixed 5.5 h after infection, and infectivity was assessed by microscopy-based quantification of NP-positive cells. Curves are derived from three independent experiments, and error bars represent SD. **(d)** Predicted inhibition curves of antibodies inhibiting viral fusion for IAV with regular trimer number (300 trimers/virion, black line) and reduced trimer number (219 trimers/virion, red line). **(e and f)** IAV A/WSN/33 produced in A549 control or A549-IFITM3 cells was input normalized by RT-qPCR and incubated with different dilutions of the broadly neutralizing stem-specific monoclonal antibody mAb 1.12 (e) or the broadly neutralizing stem-specific monoclonal antibody mAb 3.1 (f) before being used for infecting MDCKII cells. Cells were fixed 5.5 h after infection and infectivity was assessed by microscopy-based quantification of NP-positive cells. Curves are derived from three independent experiments, and error bars represent SD. **(g–i)** IAV strain A/Netherlands/602/2009 (A/Neth/09) produced in MDCK control or MDCK-IFITM3 cells was input normalized and incubated with different dilutions of a monoclonal anti-A/Neth/09 HA antibody (g) or two different polyclonal human sera from individuals vaccinated against pandemic 2009 IAV (h and i) before being used to infect MDCK cells. Cells were lysed 7 h after infection and infectivity was assessed by RT-qPCR for the M segment. Curves are derived from three independent experiments, and error bars represent SD.

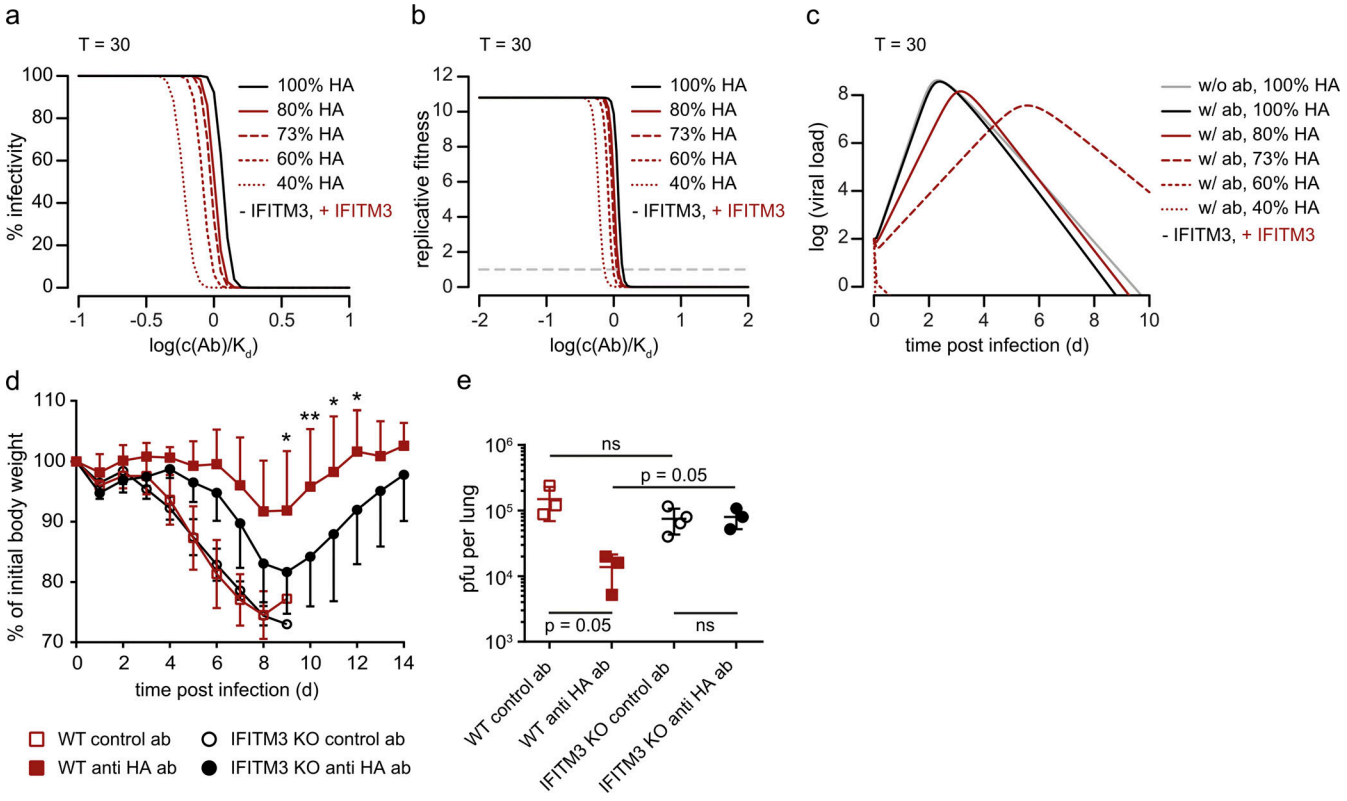

Figure 5. **IFITM3 sensitizes IAV to antibody-mediated neutralization in vivo. (a)** Predicted inhibition curves of antibodies interfering with IAV binding to host cells for IAV with regular trimer number (300 trimers/virion, black line) and reduced trimer numbers (reduction to 80%, 73%, 60%, and 40% HA content, red lines). **(b)** Predicted replicative fitness of IAV with regular trimer number (300 trimers/virion, black line) and reduced trimer numbers (reduction to 80%, 73%, 60%, and 40% HA content, red lines) as a function of antibody concentrations. Modeling was performed for antibodies inhibiting virus binding to host cells. **(c)** Predicted virus dynamics in the presence of antibodies acting on the stage of binding for virus stocks with and without IFITM3 incorporation. The antibody concentration was chosen such that the fitness difference for virus stocks with and without IFITM3 incorporation is maximal. **(d)** Morbidity after lethal challenge with PR8 virus (80 PFU) in the presence of a low dose of a PR8 HA head-specific monoclonal antibody (0.375 mg/kg) or a control antibody. Error bars represent SD. Statistically significant differences due to the absence of IFITM3 in mice that received PR8 HA head-specific antibody treatment (n = 7–9 mice/group) were assessed by two-way ANOVA with repeated measures. *, $P < 0.05$; **, $P < 0.01$. **(e)** Lung virus titers at 6 d after infection with PR8 virus are reduced by a low dose of a PR8 HA head-specific monoclonal antibody in WT but not in IFITM3 knockout mice (n = 3–4 mice/group). Error bars represent SD. Statistical significance was assessed by a one-sided Wilcoxon rank sum test. Note that with sample sizes of three data points per group, the smallest P value possible in a Wilcoxon rank sum test is $P = 0.05$.

the IFITM3-mediated reduction in HA content of IAV virions is relevant in vivo.

To formally evaluate the role of IFITM3-mediated reduction in IAV HA content and its effects on antibody neutralization, we employed a mouse model for IAV infection and pathogenesis in which the direct antiviral activity of IFITM3 on virus entry is not protective: Upon infection of mice with 80 PFU of IAV strain A/PR/8/34 (PR8), no reduction in viral titers or protection from weight loss can be observed in WT mice compared with IFITM3 knockout mice, even though high IFITM3 levels can be observed in the lungs of infected WT mice (Fig. S5 a; Lange et al., 2008). When using these conditions in combination with pretreatment with an irrelevant antibody, IFITM3 knockout and WT mice similarly succumbed to infection by day 9 (Fig. 5 d, open symbols) and no significant difference in viral titers in the lung was noted (Fig. 5 e, open symbols). In contrast, when mice were pretreated with a low dose of a PR8 HA head-specific monoclonal antibody, mimicking suboptimal antibody concentrations from previous infections or vaccinations, we observed a clear difference between WT and IFITM3 knockout mice: Viral titers were reduced 10-fold by the antibody pretreatment in WT animals (Fig. 5 e, red symbols), but no effect of the antibody was seen in IFITM3 knockout mice (Fig. 5 e, black symbols). This resulted in strong antibody-mediated protection from weight loss in WT animals, but significantly less protection in IFITM3 knockout mice (Fig. 5 d, filled symbols). A control experiment with a high dose of the same antibody showed that complete protection was possible in both groups of mice (Fig. S5 b). While we were unable to purify IAV from infected mouse lungs to analyze HA levels, our data still validate the modeling results and show that IFITM3 substantially impacts the outcome of an IAV infection when suboptimal levels of neutralizing antibodies are present, likely through a reduction in viral HA content. Scenarios where this would be highly relevant would be when antibody titers are waning after vaccination, or when antibodies induced by infections with previous strains of IAV display low cross-reactivity to a new strain of IAV.

Discussion

IFITM proteins are potent antiviral mediators of the IFN response that have been identified in many species (Bailey et al., 2012; Benfield et al., 2015; Brass et al., 2009; Lanz et al., 2015; Smith et al., 2013). Early on, it was observed that expression of IFITMs in viral target cells blocks virus entry, but only later was it established that IFITMs can also become incorporated into newly budded virus particles and negatively impact virus infectivity (Compton et al., 2014; Feeley et al., 2011; Tartour et al., 2014; Tartour et al., 2017; Yu et al., 2015). Here, we reveal yet another mode of viral inhibition by IFITM3 in which incorporation of human IFITM3 into IAV particles sensitizes the virus to antibody-mediated neutralization.

Using HIV-1–based PV- and IAV-based VLP systems, we demonstrate that IFITM3 can compete with IAV glycoproteins for incorporation and thereby reduce the amount of HA present in PVs or VLPs, which leads to reduced infectivity. As we also observed reduced IAV-VLP infectivity when IFITM1 was coexpressed in producer cells, we speculate that this antiviral mechanism could be shared by other IFITM proteins. Given that proximity of IFITM localization and VLP assembly sites would be a prerequisite for competition, these data support the model suggested by Tartour et al. (2017) that the site of virus assembly determines sensitivity to IFITM-mediated imprinting of virus infectivity. For HIV and MLV, two mechanisms seem to contribute to the reduction in infectivity when virus particles are produced in IFITM3-expressing cells, the IFITM3-mediated reduction of total envelope protein levels in the producer cell, and the reduced fusogenicity of the IFITM3-containing particles, probably due to IFITM3-mediated decreased membrane fluidity (Ahi et al., 2020; Compton et al., 2014; Tartour et al., 2017). For authentic IAV particles, we did not observe an IFITM3-mediated reduction of total HA levels in the producer cell. Instead, the reduction in HA levels was specific to incorporation into virus particles. This could either be explained by competition for space at the budding sites of IAV or by IFITM3-mediated increased membrane rigidity at the budding sites that impacts incorporation of IAV glycoproteins. Given that ectopic expression of EGFR did not lead to the same phenotype, a simple competition with any plasma membrane protein can be excluded; however, competition for a specific subdomain of the membrane that can be occupied by both HA and IFITM3, but not EGFR, is still a possible mechanism. Alternatively, higher membrane rigidity induced by IFITM3 could affect HA incorporation by an unknown mechanism, thereby causing the observed decrease in virion HA levels. The reduction in VLP or PV infectivity would then result from lower HA levels and possibly also reduced membrane fluidity during fusion.

Importantly, we also show that authentic IAV incorporates IFITM3 and displays a reduction in HA levels as observed in the PV and IAV-VLP system; however, the infectivity of authentic IAV was not affected. The fact that we observed higher HA:M1 ratios in IAV particles compared with IAV-VLPs suggests that the high number of HA trimers on IAV renders the virus insensitive to direct IFITM3-mediated loss of infectivity. It is thus tempting to speculate that IFITM restriction has contributed to the evolution of the high glycoprotein density on IAV.

The observation that HA levels are reduced by IFITM3, but without a consequent direct loss of infectivity, prompted us to investigate whether the decreased HA levels render the virus more sensitive to antibody-mediated neutralization. Indeed, our mathematical modeling results and neutralization analysis revealed that this was the case, uncovering a hitherto unknown mechanism of virus inhibition supported by IFITM proteins. Of note, the increased sensitivity was only observed for antibodies that act on virus binding, but not for HA-stem–directed antibodies that only block viral fusion. This can be explained by the fact that ∼20 to 30 HA trimers are required for virus binding, whereas three to four trimers are sufficient for fusion (Danieli et al., 1996; Floyd et al., 2008; Ivanovic et al., 2013). A reduction in trimer number would therefore affect virus binding substantially more than the fusion process.

When we employed modeling approaches to assess replicative fitness, we found that the reduction in virion-associated HA levels was predicted to affect viral fitness. Importantly, the mathematical modeling for viral dynamics in vivo in the presence of antibodies targeting virus binding predicted a 10-fold decrease and a delay of 4 d in peak virus titer. Using a mouse model and a viral infectious dose in which the direct antiviral activity of IFITM3 does not significantly protect mice, we show that, indeed, a low dose of an HA-specific antibody can still protect WT mice, but not IFITM3 knockout mice. Our results thus suggest an important role for IFITM3 in secondary influenza virus infections, when antibodies would be present that can confer some degree of protection. For example, infection with viruses of the same subtype that are a few influenza seasons apart could provide such a scenario in which antibodies are present that bind the virus, but only neutralize with low efficiency. Here, it could be particularly relevant that IFITM3 sensitizes IAV for antibody-mediated neutralization, thereby enhancing the efficiency of the antibody response. As we observed only minor changes in neutralization sensitivity when using stem-directed antibodies, the IFITM3-triggered enhancement of the antibody activity would probably be less relevant in infections with IAV subtypes where cross-neutralization is largely observed for stem-directed antibodies.

Thus far, several studies have reported a link between the *IFITM3* gene and the outcome of influenza virus infection in vivo. Specifically, it was shown that IFITM3 polymorphism rs12252-C, which was reported to code for an N-terminally truncated inactive form of IFITM3, contributes to poor clinical outcomes in patients infected with the 2009 pandemic H1N1 (Everitt et al., 2012; Zhang et al., 2013); however, this association could not be confirmed in other cohorts, and evidence has been presented that the N-terminally truncated version of IFITM3 still possesses antiviral activity (Mills et al., 2014; Randolph et al., 2017; Williams et al., 2014). Furthermore, the single-nucleotide polymorphism rs34481144, located in the *IFITM3* promoter region, was identified as a novel genetic determinant of severe outcomes of IAV infection in humans (Allen et al., 2017). In line with a previous study that highlighted a role for IFITM3 in protecting lung resident memory T cells from IAV infection in mice, the risk-conferring allele was associated with lower numbers of $CD8^+$ T cells in the airways of IAV-infected

patients (Allen et al., 2017; Wakim et al., 2013). Moreover, a recent study identified IFITM3 as a regulator of phosphoinositide-3-kinase signaling in B cells, which is required for efficient expansion of B cells with high affinity to antigen (Lee et al., 2020). Taken together, there is ample support for a protective role of IFITM3 against IAV infection in vivo, and evidence is accumulating that IFITM3 is not only part of the early IFN-mediated response but also shapes the adaptive immune response.

Here, we reveal that IFITM3 can also impact the functional antibody response to IAV. Specifically, we demonstrate that IFITM3 can compete with the viral glycoproteins for incorporation into IAV, which leads to reduced levels of HA in viral particles. As IAV displays high HA density on its surface, the observed reduction was not sufficient to directly impact IAV infectivity; however, the IFITM3-induced decrease in viral HA content sensitizes the virus for antibody-mediated neutralization, which can affect the outcome of infection in vivo. This novel link between the innate restriction factor IFITM3 and the humoral immune response will be relevant for the development and efficacy assessment of novel seasonal and pandemic vaccines.

Materials and methods

Cell lines

HEK 293T, A549, TZM-bl, and MDCKII cells were maintained in DMEM supplemented with 10% FCS (Thermo Fisher Scientific) and penicillin-streptomycin (100 U/ml; Thermo Fisher Scientific). Human IFITM3 was amplified from cDNA extracted from IFN-α–stimulated A549 cells using the following primers: 5′-GACAGA ATTCATGGACTACAAAGACGATGACGATAAAAATCACACTGT CCAAA-3′ (forward) and 5′-GACACTCGAGCTATCCATAGGCCT GGAA-3′ (reverse). After restriction digest by EcoRI and XhoI, the IFITM3 PCR product was ligated into the pLVX-IRES-Puromycin vector plasmid (Clontech) to yield pLVX-Flag-IFITM3. Untagged human IFITM3 was amplified from pLVX-Flag-IFITM3 and cloned with EcoRI and NotI into pLVX-IRES-Puromycin (Clontech). To generate lentiviral particles, 293Ts were cotransfected with pCMVdR8.91, pMD2.G and pLVX empty vector, pLVX-Flag-IFITM3, or pLVX-IFITM3 for 48 h before harvesting of supernatants, filtration through a 0.45-µM filter, and transduction of cells in the presence of polybrene (final concentration of 8 µg/ml; Sigma-Aldrich). Two days later, transduced cells were selected with puromycin (Thermo Fisher Scientific). A549 control, A549-Flag-IFITM3, TZM-bl control, and TZM-bl-Flag-IFITM3 cells were subcloned by limiting dilution as expression levels of IFITM3 were not homogenous after initial transduction. MDCK control and MDCK-IFITM3 cells were used as bulk population after transduction as IFITM3 expression was homogenous.

HIV-1–based PV production, purification, and infection

HIV-1–based PVs with either the HIV-1 JRFL, IAV A/WSN/33, or VSV envelope glycoproteins were generated by transfecting HEK 293T cells with pNLLuc-AM (Pugach et al., 2007), envelope expression plasmids, and pCAGGS-Flag-IFITM3 or the empty vector pCAGGS for the production of PV in the absence of IFITM3 or pcDNA6A-myc-EGFR (a kind gift from Mien-Chie Hung, University of Texas M.D. Anderson Cancer Center, Houston, TX; Addgene plasmid #42665; Hsu and Hung, 2007). PVs were harvested 72 h after transfection and their concentration was determined by an in-house p24 ELISA. A549 or TZM-bl cells seeded into 96-well plates were infected with PVs at an equivalent of 3 ng p24/well for 90 min in the presence of diethylaminoethyl-dextran (150 µg/ml; Sigma-Aldrich) before the inoculum was removed and replaced by DMEM supplemented with 10% FCS and penicillin-streptomycin (100 U/ml). PV infectivity was measured 48 h after infection by quantifying firefly luciferase activity using the ONE-Glo Luciferase Assay System (Promega) according to the manufacturer's protocol. For analysis of PVs by Western blot, PVs were purified as follows: After an initial centrifugation at 1,500 ×*g* for 5 min to remove cellular debris, PV-containing supernatant was filtered through a 0.45-µm filter. To achieve a more stringent removal of cellular debris, supernatant was ultracentrifuged at 10,000 rpm at 4°C for 20 min, before ultracentrifugation of VLPs through a 20% (wt/vol) sucrose cushion in NTE buffer (100 mM NaCl, 10 mM Tris-HCl [pH 7.5], 1 mM EDTA [pH 8]) at 25,000 rpm for 90 min. Supernatant was decanted and the PV pellet dissolved in Opti-MEM (Gibco) at 4°C overnight.

IAV-VLP production, normalization, and infection

VLPs harboring BlaM1 fusion proteins were produced essentially as described before (Tscherne et al., 2010). Briefly, HEK 293T cells seeded onto poly-L-lysine–coated (Sigma-Aldrich) 6-well plates were transfected in Opti-MEM (Gibco) with 2.5 µg BlaM1, 500 ng pCAGGS-WSN-HA, 1.125 µg pCAGGS-WSN-NA, 250 ng pCAGGS-WSN-M2, and 300 ng pCAGGS-IFITM3, pCAGGS-IFITM1, or pCAGGS per well using ViaFect (Promega) as the transfection reagent (2.5 µl ViaFect/µg DNA). Medium was exchanged 8 h after transfection. VLPs were harvested 72 h after transfection and treated with 6 µg/ml N-tosyl-L-phenylalanine chloromethyl ketone trypsin (Sigma-Aldrich) for efficient HA cleavage. For infection of MDCKII, MDCK control, or MDCK-IFITM3 cells, IAV-VLP input was normalized by Western blotting for BlaM1 using the mouse monoclonal anti-IAV M1 (HB-64; American Type Culture Collection) antibody. At 4 h after infection, cells were harvested by trypsinization and incubated with the fluorogenic substrate CCF2-AM (Thermo Fisher Scientific). Cells were analyzed on a FACSVerse System (BD Biosciences) and dead cells were excluded by a live/dead staining (LIVE/DEAD Fixable Near-IR Dead Cell Stain Kit; Thermo Fisher Scientific).

IAV infections in vitro

Cells were washed with PBS before infection. IAV A/WSN/33 or A/Netherlands/602/2009 was diluted appropriately in PBS supplemented with 2 mM Mg^{2+}, 1 mM Ca^{2+}, 0.3% BSA, and 1% penicillin-streptomycin (infection PBS). Infection was performed at 37°C for 1 h. Thereafter, virus inoculum was removed and cells were washed with PBS before DMEM containing 20 mM Hepes, 0.3% BSA, and 1% penicillin-streptomycin (postinfection DMEM) was added to the cells. Virus was

grown in the presence of 1 µg/ml N-tosyl-L-phenylalanine chloromethyl ketone trypsin (Sigma-Aldrich) for 48–72 h.

To normalize viral input in subsequent infectivity assays, quantitative PCR (qPCR) on the viral M segment was performed. Viral RNA was extracted using the QIAamp Viral RNA Kit (Qiagen) and cDNA synthesized by the SuperScript III Reverse transcription (Thermo Fisher Scientific) using random primers (Promega). qPCR for the M segment was performed using EvaGreen Master Mix for qPCR (Biotium) with the following primers: 5′-GCAGCAGAGGCCATGGATATTG-3′ (forward) and 5′-TTTGCT GCAATGACGAGAGGATC-3′ (reverse). Virus grown on control or IFITM3-expressing A549 cells was diluted according to qPCR results for all infectivity assays.

Virus infectivity was measured in an IAV reporter assay. Briefly, HEK 293T cells seeded into 96-well plates were transfected with 20 ng/well of an IAV reporter plasmid encoding firefly luciferase in complementary reverse orientation, flanked by IAV noncoding regions, thus mimicking an IAV segment. At 24 h after transfection, cells were infected with A/WSN/33 at an MOI of 0.3. At 24 h after infection, luciferase activity was measured using the ONE-Glo luciferase assay substrate (Promega) according to manufacturer's protocols.

To assess IFITM incorporation into IAV by Western blotting, virus was purified as described for PV and subjected to Western blotting as described below.

Western blotting

To prepare cell extracts, cells were lysed in 1× Laemmli buffer (62.5 mM Tris-HCl [pH 6.8], 10% glycerol, 2% SDS, 100 mM dithiothreitol, 0.02% bromophenol blue). Viruses, VLPs, and lung homogenates were mixed with 5× Laemmli buffer to obtain 1× Laemmli buffer lysates. Samples were run on SDS-PAGE gels and blotted onto nitrocellulose membranes (Hybond ECL; GE Healthcare). All stainings were performed in Tris-buffered saline mixed with 0.5% Tween-20 (Sigma-Aldrich) and 3% powdered milk. The following antibodies were used: mouse monoclonal anti-Flag (clone M2; Sigma-Aldrich), rabbit polyclonal anti-IFITM3 (Proteintech), mouse monoclonal anti–β-actin (Santa Cruz Biotechnology), mouse monoclonal anti–HIV-1 p24 (ab9071; Abcam), mouse monoclonal anti-IAV M1 (HB-64; American Type Culture Collection), rabbit polyclonal anti-nucleoprotein (NP; a kind gift of A. Nieto, Spanish National Center for Biotechnology, Madrid, Spain), mouse monoclonal anti-A/WSN/33 HA (clone H15-B9-22 from Wistar), rabbit polyclonal anti-A/WSN/33, and mouse monoclonal anti-A/Netherlands/602/2009 HA clone 31C2 (Manicassamy et al., 2010). Secondary antibody staining was performed using near-infrared fluorescent secondary antibodies (Li-Cor) and images were acquired on an Odissey Fc imaging system. Western blot signal intensities were quantified using the Image Studio software (Li-Cor).

NA assay

NA activity was measured using the NA-Star Influenza Neuraminidase Inhibitor Resistance Detection Kit (Applied Biosystems) according to the manufacturer's instructions.

IF staining

For IF analysis of HA and IFITM3 localization, A549 or 293T cells were grown on glass coverslips in 24-well plates. Cells were either transfected with expression plasmids for HA (A/WSN/33) and IFITM3 for 24 h or infected with A/WSN/33 (MOI 1) for 16 h. Cells were fixed with 3% paraformaldehyde for 15 min, washed, and permeabilized using IF buffer (PBS supplemented with 50 mM NH_4Cl, 0.1% saponin, and 2% BSA). Cells were incubated for 1 h at room temperature with primary antibodies (rabbit polyclonal anti-IFITM3 and mouse monoclonal anti-A/WSN/33 HA clone H15-B9-22) and washed three times with IF buffer before secondary antibodies (A-21202 and A10040; Life Technologies) were added for 1 h at room temperature. Cells were washed three times with IF buffer, inversely mounted onto glass microscope slides using DAPI Fluoromount G (#0100-20; Southern Biotech), and images were acquired with a confocal laser scanning microscope (Leica SP5).

Transmission electron microscopy of immunogold-labeled viral particles

Viral particles were purified as described above. Carbon-coated nickel grids were glow discharged before purified viral particle solution was applied. Samples were fixed with 4% paraformaldehyde in 0.1 M Hepes for 7 min. After one short wash in PBS, samples were permeabilized with 0.5% Triton X-100 in PBS for 1 min and washed again three times in PBS. Free aldehydes were quenched with 0.15% glycine in PBS. To prevent unspecific antibody binding, samples were blocked in 1% BSA (Merck) in PBS. Primary antibody staining was performed using rabbit polyclonal anti-IFITM3 antibody (Proteintech) diluted in 1% BSA in PBS. Samples were washed three times in 1% BSA in PBS, before secondary antibody staining was performed using a goat anti-mouse IgG Gold antibody (Sigma-Aldrich) at an OD of 0.15. After secondary antibody staining, samples were washed in PBS and fixed in 4% paraformaldehyde in 0.1 M Hepes, before being negatively stained with 1% uranyl acetate and imaged in a Philips CM100 transmission electron microscope operated at 100 kV.

Neutralization assay

The following antibodies/sera were used in neutralization assays with A/WSN/33: mouse monoclonal anti-A/WSN/33 HA (clone H15-B9-22 from Wistar), rabbit polyclonal anti-A/WSN/33, and the human monoclonal heterosubtypic antibodies mAb 3.1 and mAb 1.12 (Wyrzucki et al., 2015; Wyrzucki et al., 2014), a kind gift from L. Hangartner (The Scripps Research Institute, La Jolla, CA). The following antibodies/sera were used in neutralization assays with A/Netherlands/602/2009: mouse monoclonal anti-A/Netherlands/602/2009 HA clone 31C2 (Manicassamy et al., 2010), human convalescent sera to 2009 H1N1 Influenza A Virus NR-18964 (BEI Resources, National Institute of Allergy and Infectious Diseases, National Institutes of Health), and NR-18965 (BEI Resources, National Institute of Allergy and Infectious Diseases, National Institutes of Health).

IAV A/WSN/33 grown on control or IFITM3-expressing A549 cells was diluted in postinfection DMEM to an MOI of 4 and incubated with different dilutions of antibodies or serum for 1 h

at 4°C. MDCKII cells seeded in 96-well plates were infected with the inoculum at 37°C and 5% CO_2. At 5.5 h after infection, cells were washed three times with PBS and fixed using 3% paraformaldehyde. To permeabilize the fixed cells, 0.5% Triton X-100 in PBS was added for 5 min at room temperature. Cells were washed three times with PBS before being incubated for 1 h at room temperature with the primary antibody (mouse monoclonal anti-NP antibody). After three washing steps with PBS, the secondary antibody (A-21202; Life Technologies) was added to the cells for 1 h at room temperature. The number of NP-positive cells was quantified using the IncuCyte ZOOM system (Essen BioScience).

Neutralization assays with IAV A/Netherlands/602/2009 were done by RT-qPCR as described by Teferedegne et al. (2013) using the matrix (M) gene specific primers M30F2 5′-ATGAGY CTTYTAACCGAGGTCGAAACG-3′ and M264R3 5′-TGGACAAAN CGTCTACGCTGCAG-3′, recommended by the World Health Organization. In brief, IAV A/Netherlands/602/2009 was grown on control or IFITM3-expressing MDCK cells and diluted in postinfection DMEM to an MOI of 1. Viruses were incubated with increasing concentrations of antibody or serum for 1 h at 37°C. 30,000 MDCK cells were infected in suspension with the preincubated virus for 7 h at 37°C. Cells were washed once with PBS and lysed with 100 µl iScript RT-qPCR Sample Preparation Reagent (catalog #1708899; Bio-Rad) for 2 min at room temperature. 1 µl of the respective RNA extract was used as input for a 10 µl RT-qPCR reaction using iTaq Universal SYBR Green One-Step Kit (catalog #1725151; Bio-Rad) according to the manufacturer's protocol. Reactions were measured using a 7300 Real-Time PCR System from Applied Biosystems.

Modeling

Antibody neutralization curves were predicted as described in Brandenberg et al. (2017), with 300 trimers per virion for IAV produced in the absence of IFITM3 and 219 trimers per virion for IAV produced in the presence of IFITM3. The reduction in trimer content is based on the 27% reduction observed in our experiments (Fig. 3 b). We set the reaction constant to $K_D = 10^{-9}$. The model was implemented in the statistical software R and is available upon request. We fitted a hill curve to these inhibition curves using a nonlinear least square algorithm to estimate the concentration that leads to 50% inhibition (IC50) and slope values. To predict the effect of varying inhibitory concentrations for virion populations with and without IFITM3 incorporation on the replicative fitness, we adapted a framework previously established for HIV-1 (Magnus et al., 2016). In short, the replicative fitness, F, as a function of varying antibody concentrations, cAb, is

$$F(cAb) = F_0 \Big/ \left(1 + \left(\frac{cAb}{IC50}\right)^m\right).$$

We used the previously described replicative fitness for IAV of $F_0 = 10.8$ as the baseline fitness F_0 in absence of antibodies (Baccam et al., 2006). The virus dynamics of IAV were modeled according to the target cell–limited model established by Baccam et al. (2006), which describes the change of uninfected cells, U, infected cells, I, and virions, V:

$$\frac{dU}{dt} = -\beta UV,$$
$$\frac{dI}{dt} = \beta UV - \delta I,$$
$$\frac{dV}{dt} = pI - cV.$$

In this system of ordinary differential equations (ODEs), $\beta = 2.7 \times 10^{-5}$ ml/(TCID50 d) is the infection rate, $\delta = 4\ d^{-1}$ is the death rate of infected cells, and $P = 1.2 \times 10^{-2}$ TCID50/(ml d) is the virion production rate. The infection is started with $V_0 = 9.3 \times 10^{-2}$, and $U_0 = 4 \times 10^8$ uninfected target cells. These values are based on estimates in Baccam et al. (2006). TCID50 was set to 1,000 virions. The replicative fitness F in this model is defined by the parameters in the system of ODEs $F = (p\beta U_0)/(c\delta)$.

We model neutralization as increased virion death rate, c, by transforming the above equation of the replicative fitness to $c = (p\beta U_0)/(F\delta)$. With this parameterization, we numerically calculated the above system of ordinary differential equations using the function ode() of the R package deSolve.

Mouse experiments

All mouse procedures performed were approved in advance by the Icahn School of Medicine at Mount Sinai Institutional Animal Care and Use Committee in accordance with the guidelines stated in the Guide for the Care and Use of Laboratory Animals. IFITM3 knockout mice were a kind gift from Dr. Michael Farzan (Harvard Medical School, Boston, MA). Generation of IFITM3 knockout mice by insertion of the gene encoding eGFP in exon 1 of the IFITM3 gene is described in Lange et al. (2008). Age-matched female C57BL/6 mice (Charles River Laboratories) were used as WT controls. Mice were arbitrarily assigned to study groups and had free access to food and sterilized tap water.

PY102 is a monoclonal antibody of the IgG1 subtype produced by the Center for Therapeutic Antibody Development at the Icahn School of Medicine at Mount Sinai. PY102 binds the HA head of PR8 H1N1 virus (Reale et al., 1986). A low (0.375 mg/kg) or high (2.5 mg/kg) dose of monoclonal antibody PY102 was prepared in 100 µl vol/mouse in PBS and injected i.p. 4 h before influenza virus challenge.

For challenge with influenza PR8 H1N1 virus, mice were mildly sedated by i.p. injection of a ketamine/xylazine mixture and challenged intranasally with 80 PFU of virus diluted in 50 µl PBS. Body weight was monitored daily for 14 d. Mice that lost more than 25% of their initial body weight were euthanized.

To determine lung virus titers or analyze IFITM3 expression levels, lungs were removed aseptically and homogenized in 1 ml PBS in a Benchmark BeadBlaster24 (Benchmark Scientific). The homogenates were centrifuged (15 min, 16,100 ×*g*, 4°C) to remove cellular debris and stored at −80°C. Titers of infectious virus were determined by plaque assay. Briefly, 250 µl of 10-fold dilutions of lungs homogenized in PBS were used to infect confluent monolayers of MDCK cells. Virus was allowed to attach to MDCK cells for 1 h at 37°C. Cells were washed once with PBS and overlayed with oxoid agar (Oxoid) prepared using $NaHCO_3$-buffered serum-free 2× Minimum Essential Medium (MEM)/BSA containing diethylaminoethyl-dextran and supplemented with tosyl phenylalanyl chloromethyl ketone–treated

trypsin (Sigma-Aldrich). Cells were incubated at 37°C for 48 h. PFUs were determined by staining viral antigen with 1/1,000 diluted postchallenge serum followed by incubation with HRP-labeled sheep anti-mouse serum (1/1,000 dilution; GE Healthcare) and TrueBlue substrate (KPL-Seracare).

Online supplemental material

Fig. S1 shows that IFITM3 reduces PV infectivity at the level of producer and target cell for IAV and HIV-1 but not for VSV in an HIV-1–based PV system. Fig. S2 illustrates how PV^{HIV} and PV^{IAV} display decreased glycoprotein levels when produced in IFITM3-expressing cells but not in EGFR-expressing cells. Fig. S3 shows that IFITM3 expression does not lead to reduced cellular HA levels and that IFITM3 shares the ability to reduce IAV-VLP infectivity with IFITM1. Fig. S4 illustrates IFITM3 expression to similar levels in A549-IFITM3 and IFN-treated A549 cells and colocalization with HA during IAV infection. Fig. S5 shows how a high dose of an HA head-specific antibody can protect WT and IFITM3 knockout mice from disease.

Acknowledgments

We thank Richard Cadagan for excellent technical assistance. Imaging was performed with equipment and support of the Center for Microscopy and Image Analysis, University of Zurich. C. Magnus is grateful to Janina Linnik for helpful comments on the mathematical analysis. The graphical abstract was created with BioRender.com.

This work was supported by the Swiss National Science Foundation (grant 31003A_176170 to S. Stertz; grant 314730_172790 to A. Trkola; and grant 31003A_182464 to B.G. Hale) and the Hartmann Müller Foundation (grant 2038 to S. Stertz). This work was also partly supported by National Institutes of Health grants U19AI117873 and P01AI097092 and by the Center for Research on Influenza Pathogenesis, a National Institute of Allergy and Infectious Diseases–funded Center of Excellence for Influenza Research and Surveillance (contract no. HHSN272201400008C) to A. García-Sastre.

Author contributions: Conceptualization: C. Lanz, M. Schotsaert, B.G. Hale, A. Trkola, A. García-Sastre, and S. Stertz; investigation: C. Lanz, M. Schotsaert, C. Magnus, U. Karakus, A. Hunziker, M.S. Borau, C. Martínez-Romero, E.E. Spieler, and E. Moritz; writing – original draft: C. Lanz, M. Schotsaert, C. Magnus, U. Karakus, A. Hunziker, M.S. Borau, S.C. Günther, and S. Stertz; writing – review and editing: C. Lanz, M. Schotsaert, C. Magnus, U. Karakus, A. Hunziker, M.S. Borau, C. Martínez-Romero, E.E. Spieler, S.C. Günther, B.G. Hale, A. Trkola, A. García-Sastre, and S. Stertz; funding acquisition: B.G. Hale, A. Trkola, A. García-Sastre, and S. Stertz; supervision: B.G. Hale, A. Trkola, A. García-Sastre, and S. Stertz.

Disclosures: The authors declare no competing interests exist.

Submitted: 19 February 2020
Revised: 2 February 2021
Accepted: 4 March 2021

References

Ahi, Y.S., D. Yimer, G. Shi, S. Majdoul, K. Rahman, A. Rein, and A.A. Compton. 2020. IFITM3 Reduces Retroviral Envelope Abundance and Function and Is Counteracted by glycoGag. *MBio.* 11:e03088-19. https://doi.org/10.1128/mBio.03088-19

Allen, E.K., A.G. Randolph, T. Bhangale, P. Dogra, M. Ohlson, C.M. Oshansky, A.E. Zamora, J.P. Shannon, D. Finkelstein, A. Dressen, et al. 2017. SNP-mediated disruption of CTCF binding at the IFITM3 promoter is associated with risk of severe influenza in humans. *Nat. Med.* 23:975–983. https://doi.org/10.1038/nm.4370

Appourchaux, R., M. Delpeuch, L. Zhong, J. Burlaud-Gaillard, K. Tartour, G. Savidis, A. Brass, L. Etienne, P. Roingeard, and A. Cimarelli. 2019. Functional Mapping of Regions Involved in the Negative Imprinting of Virion Particle Infectivity and in Target Cell Protection by Interferon-Induced Transmembrane Protein 3 against HIV-1. *J. Virol.* 93:e01716-18. https://doi.org/10.1128/JVI.01716-18

Baccam, P., C. Beauchemin, C.A. Macken, F.G. Hayden, and A.S. Perelson. 2006. Kinetics of influenza A virus infection in humans. *J. Virol.* 80: 7590–7599. https://doi.org/10.1128/JVI.01623-05

Bailey, C.C., I.C. Huang, C. Kam, and M. Farzan. 2012. Ifitm3 limits the severity of acute influenza in mice. *PLoS Pathog.* 8:e1002909. https://doi.org/10.1371/journal.ppat.1002909

Benfield, C.T.O., S.E. Smith, E. Wright, R.S. Wash, F. Ferrara, N.J. Temperton, and P. Kellam. 2015. Bat and pig IFN-induced transmembrane protein 3 restrict cell entry by influenza virus and lyssaviruses. *J. Gen. Virol.* 96: 991–1005. https://doi.org/10.1099/vir.0.000058

Brandenberg, O.F., C. Magnus, P. Rusert, H.F. Günthard, R.R. Regoes, and A. Trkola. 2017. Predicting HIV-1 transmission and antibody neutralization efficacy in vivo from stoichiometric parameters. *PLoS Pathog.* 13: e1006313. https://doi.org/10.1371/journal.ppat.1006313

Brass, A.L., I.C. Huang, Y. Benita, S.P. John, M.N. Krishnan, E.M. Feeley, B.J. Ryan, J.L. Weyer, L. van der Weyden, E. Fikrig, et al. 2009. The IFITM proteins mediate cellular resistance to influenza A H1N1 virus, West Nile virus, and dengue virus. *Cell.* 139:1243–1254. https://doi.org/10.1016/j.cell.2009.12.017

Compton, A.A., T. Bruel, F. Porrot, A. Mallet, M. Sachse, M. Euvrard, C. Liang, N. Casartelli, and O. Schwartz. 2014. IFITM proteins incorporated into HIV-1 virions impair viral fusion and spread. *Cell Host Microbe.* 16: 736–747. https://doi.org/10.1016/j.chom.2014.11.001

Compton, A.A., N. Roy, F. Porrot, A. Billet, N. Casartelli, J.S. Yount, C. Liang, and O. Schwartz. 2016. Natural mutations in IFITM3 modulate post-translational regulation and toggle antiviral specificity. *EMBO Rep.* 17: 1657–1671. https://doi.org/10.15252/embr.201642771

Danieli, T., S.L. Pelletier, Y.I. Henis, and J.M. White. 1996. Membrane fusion mediated by the influenza virus hemagglutinin requires the concerted action of at least three hemagglutinin trimers. *J. Cell Biol.* 133:559–569. https://doi.org/10.1083/jcb.133.3.559

Domingues, P., D. Eletto, C. Magnus, H.L. Turkington, S. Schmutz, O. Zagordi, M. Lenk, M. Beer, S. Stertz, and B.G. Hale. 2019. Profiling host ANP32A splicing landscapes to predict influenza A virus polymerase adaptation. *Nat. Commun.* 10:3396. https://doi.org/10.1038/s41467-019-11388-2

Everitt, A.R., S. Clare, T. Pertel, S.P. John, R.S. Wash, S.E. Smith, C.R. Chin, E.M. Feeley, J.S. Sims, D.J. Adams, et al. MOSAIC Investigators. 2012. IFITM3 restricts the morbidity and mortality associated with influenza. *Nature.* 484:519–523. https://doi.org/10.1038/nature10921

Feeley, E.M., J.S. Sims, S.P. John, C.R. Chin, T. Pertel, L.M. Chen, G.D. Gaiha, B.J. Ryan, R.O. Donis, S.J. Elledge, and A.L. Brass. 2011. IFITM3 inhibits influenza A virus infection by preventing cytosolic entry. *PLoS Pathog.* 7:e1002337. https://doi.org/10.1371/journal.ppat.1002337

Floyd, D.L., J.R. Ragains, J.J. Skehel, S.C. Harrison, and A.M. van Oijen. 2008. Single-particle kinetics of influenza virus membrane fusion. *Proc. Natl. Acad. Sci. USA.* 105:15382–15387. https://doi.org/10.1073/pnas.0807771105

Gorman, M.J., S. Poddar, M. Farzan, and M.S. Diamond. 2016. The Interferon-Stimulated Gene Ifitm3 Restricts West Nile Virus Infection and Pathogenesis. *J. Virol.* 90:8212–8225. https://doi.org/10.1128/JVI.00581-16

Harris, A., G. Cardone, D.C. Winkler, J.B. Heymann, M. Brecher, J.M. White, and A.C. Steven. 2006. Influenza virus pleiomorphy characterized by cryoelectron tomography. *Proc. Natl. Acad. Sci. USA.* 103:19123–19127. https://doi.org/10.1073/pnas.0607614103

Hsu, S.C., and M.C. Hung. 2007. Characterization of a novel tripartite nuclear localization sequence in the EGFR family. *J. Biol. Chem.* 282:10432–10440. https://doi.org/10.1074/jbc.M610014200

Inglis, S.C., A.R. Carroll, R.A. Lamb, and B.W. Mahy. 1976. Polypeptides specified by the influenza virus genome I. Evidence for eight distinct

gene products specified by fowl plague virus. *Virology*. 74:489–503. https://doi.org/10.1016/0042-6822(76)90355-X

Ivanovic, T., J.L. Choi, S.P. Whelan, A.M. van Oijen, and S.C. Harrison. 2013. Influenza-virus membrane fusion by cooperative fold-back of stochastically induced hemagglutinin intermediates. *eLife*. 2:e00333. https://doi.org/10.7554/eLife.00333

Jia, R., Q. Pan, S. Ding, L. Rong, S.L. Liu, Y. Geng, W. Qiao, and C. Liang. 2012. The N-terminal region of IFITM3 modulates its antiviral activity by regulating IFITM3 cellular localization. *J. Virol.* 86:13697–13707. https://doi.org/10.1128/JVI.01828-12

Jia, R., F. Xu, J. Qian, Y. Yao, C. Miao, Y.M. Zheng, S.L. Liu, F. Guo, Y. Geng, W. Qiao, and C. Liang. 2014. Identification of an endocytic signal essential for the antiviral action of IFITM3. *Cell. Microbiol.* 16:1080–1093. https://doi.org/10.1111/cmi.12262

Knossow, M., M. Gaudier, A. Douglas, B. Barrère, T. Bizebard, C. Barbey, B. Gigant, and J.J. Skehel. 2002. Mechanism of neutralization of influenza virus infectivity by antibodies. *Virology*. 302:294–298. https://doi.org/10.1006/viro.2002.1625

Lange, U.C., D.J. Adams, C. Lee, S. Barton, R. Schneider, A. Bradley, and M.A. Surani. 2008. Normal germ line establishment in mice carrying a deletion of the Ifitm/Fragilis gene family cluster. *Mol. Cell. Biol.* 28:4688–4696. https://doi.org/10.1128/MCB.00272-08

Lanz, C., E. Yángüez, D. Andenmatten, and S. Stertz. 2015. Swine interferon-inducible transmembrane proteins potently inhibit influenza A virus replication. *J. Virol.* 89:863–869. https://doi.org/10.1128/JVI.02516-14

Lee, J., M.E. Robinson, N. Ma, D. Artadji, M.A. Ahmed, G. Xiao, T. Sadras, G. Deb, J. Winchester, K.N. Cosgun, et al. 2020. IFITM3 functions as a PIP3 scaffold to amplify PI3K signalling in B cells. *Nature*. 588:491–497. https://doi.org/10.1038/s41586-020-2884-6

Li, K., R.M. Markosyan, Y.M. Zheng, O. Golfetto, B. Bungart, M. Li, S. Ding, Y. He, C. Liang, J.C. Lee, et al. 2013. IFITM proteins restrict viral membrane hemifusion. *PLoS Pathog.* 9:e1003124. https://doi.org/10.1371/journal.ppat.1003124

Lin, T.Y., C.R. Chin, A.R. Everitt, S. Clare, J.M. Perreira, G. Savidis, A.M. Aker, S.P. John, D. Sarlah, E.M. Carreira, et al. 2013. Amphotericin B increases influenza A virus infection by preventing IFITM3-mediated restriction. *Cell Rep.* 5:895–908. https://doi.org/10.1016/j.celrep.2013.10.033

Lu, J., Q. Pan, L. Rong, W. He, S.L. Liu, and C. Liang. 2011. The IFITM proteins inhibit HIV-1 infection. *J. Virol.* 85:2126–2137. https://doi.org/10.1128/JVI.01531-10

Magnus, C., L. Reh, and A. Trkola. 2016. HIV-1 resistance to neutralizing antibodies: Determination of antibody concentrations leading to escape mutant evolution. *Virus Res.* 218:57–70. https://doi.org/10.1016/j.virusres.2015.10.009

Manicassamy, B., R.A. Medina, R. Hai, T. Tsibane, S. Stertz, E. Nistal-Villán, P. Palese, C.F. Basler, and A. García-Sastre. 2010. Protection of mice against lethal challenge with 2009 H1N1 influenza A virus by 1918-like and classical swine H1N1 based vaccines. *PLoS Pathog.* 6:e1000745. https://doi.org/10.1371/journal.ppat.1000745

McMichael, T.M., L. Zhang, M. Chemudupati, J.C. Hach, A.D. Kenney, H.C. Hang, and J.S. Yount. 2017. The palmitoyltransferase ZDHHC20 enhances interferon-induced transmembrane protein 3 (IFITM3) palmitoylation and antiviral activity. *J. Biol. Chem.* 292:21517–21526. https://doi.org/10.1074/jbc.M117.800482

Mills, T.C., A. Rautanen, K.S. Elliott, T. Parks, V. Naranbhai, M.M. Ieven, C.C. Butler, P. Little, T. Verheij, C.S. Garrard, et al. 2014. IFITM3 and susceptibility to respiratory viral infections in the community. *J. Infect. Dis.* 209:1028–1031. https://doi.org/10.1093/infdis/jit468

Montefiori, D.C. 2005. Evaluating neutralizing antibodies against HIV, SIV, and SHIV in luciferase reporter gene assays. *Curr. Protoc. Immunol.* 64:12.11.1–12.11.17. https://doi.org/10.1002/0471142735.im1211s64

Otterstrom, J.J., B. Brandenburg, M.H. Koldijk, J. Juraszek, C. Tang, S. Mashaghi, T. Kwaks, J. Goudsmit, R. Vogels, R.H. Friesen, and A.M. van Oijen. 2014. Relating influenza virus membrane fusion kinetics to stoichiometry of neutralizing antibodies at the single-particle level. *Proc. Natl. Acad. Sci. USA*. 111:E5143–E5148. https://doi.org/10.1073/pnas.1411755111

Platt, E.J., K. Wehrly, S.E. Kuhmann, B. Chesebro, and D. Kabat. 1998. Effects of CCR5 and CD4 cell surface concentrations on infections by macrophagetropic isolates of human immunodeficiency virus type 1. *J. Virol.* 72:2855–2864. https://doi.org/10.1128/JVI.72.4.2855-2864.1998

Pugach, P., A.J. Marozsan, T.J. Ketas, E.L. Landes, J.P. Moore, and S.E. Kuhmann. 2007. HIV-1 clones resistant to a small molecule CCR5 inhibitor use the inhibitor-bound form of CCR5 for entry. *Virology*. 361:212–228. https://doi.org/10.1016/j.virol.2006.11.004

Rahman, K., C.A. Coomer, S. Majdoul, S.Y. Ding, S. Padilla-Parra, and A.A. Compton. 2020. Homology-guided identification of a conserved motif linking the antiviral functions of IFITM3 to its oligomeric state. *eLife*. 9:e58537. https://doi.org/10.7554/eLife.58537

Randolph, A.G., W.K. Yip, E.K. Allen, C.M. Rosenberger, A.A. Agan, S.A. Ash, Y. Zhang, T.R. Bhangale, D. Finkelstein, N.Z. Cvijanovich, et al. Pediatric Acute Lung Injury and Sepsis Investigators (PALISI) Network Pediatric Influenza (PICFLU) Investigators. 2017. Evaluation of IFITM3 rs12252 Association With Severe Pediatric Influenza Infection. *J. Infect. Dis.* 216:14–21. https://doi.org/10.1093/infdis/jix242

Reale, M.A., A.J. Manheimer, T.M. Moran, G. Norton, C.A. Bona, and J.L. Schulman. 1986. Characterization of monoclonal antibodies specific for sequential influenza A/PR/8/34 virus variants. *J. Immunol.* 137:1352–1358.

Savidis, G., J.M. Perreira, J.M. Portmann, P. Meraner, Z. Guo, S. Green, and A.L. Brass. 2016. The IFITMs Inhibit Zika Virus Replication. *Cell Rep.* 15:2323–2330. https://doi.org/10.1016/j.celrep.2016.05.074

Shi, G., A.D. Kenney, E. Kudryashova, A. Zani, L. Zhang, K.K. Lai, L. Hall-Stoodley, R.T. Robinson, D.S. Kudryashov, A.A. Compton, and J.S. Yount. 2021. Opposing activities of IFITM proteins in SARS-CoV-2 infection. *EMBO J.* 40:e106501. https://doi.org/10.15252/embj.2020106501

Smith, S.E., M.S. Gibson, R.S. Wash, F. Ferrara, E. Wright, N. Temperton, P. Kellam, and M. Fife. 2013. Chicken interferon-inducible transmembrane protein 3 restricts influenza viruses and lyssaviruses in vitro. *J. Virol.* 87:12957–12966. https://doi.org/10.1128/JVI.01443-13

Spence, J.S., R. He, H.H. Hoffmann, T. Das, E. Thinon, C.M. Rice, T. Peng, K. Chandran, and H.C. Hang. 2019. IFITM3 directly engages and shuttles incoming virus particles to lysosomes. *Nat. Chem. Biol.* 15:259–268. https://doi.org/10.1038/s41589-018-0213-2

Suddala, K.C., C.C. Lee, P. Meraner, M. Marin, R.M. Markosyan, T.M. Desai, F.S. Cohen, A.L. Brass, and G.B. Melikyan. 2019. Interferon-induced transmembrane protein 3 blocks fusion of sensitive but not resistant viruses by partitioning into virus-carrying endosomes. *PLoS Pathog.* 15:e1007532. https://doi.org/10.1371/journal.ppat.1007532

Tartour, K., R. Appourchaux, J. Gaillard, X.N. Nguyen, S. Durand, J. Turpin, E. Beaumont, E. Roch, G. Berger, R. Mahieux, et al. 2014. IFITM proteins are incorporated onto HIV-1 virion particles and negatively imprint their infectivity. *Retrovirology*. 11:103. https://doi.org/10.1186/s12977-014-0103-y

Tartour, K., X.N. Nguyen, R. Appourchaux, S. Assil, V. Barateau, L.M. Bloyet, J. Burlaud Gaillard, M.P. Confort, B. Escudero-Perez, H. Gruffat, et al. 2017. Interference with the production of infectious viral particles and bimodal inhibition of replication are broadly conserved antiviral properties of IFITMs. *PLoS Pathog.* 13:e1006610. https://doi.org/10.1371/journal.ppat.1006610

Teferedegne, B., A.M. Lewis Jr., K. Peden, and H. Murata. 2013. Development of a neutralization assay for influenza virus using an endpoint assessment based on quantitative reverse-transcription PCR. *PLoS One.* 8:e56023. https://doi.org/10.1371/journal.pone.0056023

Tscherne, D.M., B. Manicassamy, and A. García-Sastre. 2010. An enzymatic virus-like particle assay for sensitive detection of virus entry. *J. Virol. Methods.* 163:336–343. https://doi.org/10.1016/j.jviromet.2009.10.020

Wakim, L.M., N. Gupta, J.D. Mintern, and J.A. Villadangos. 2013. Enhanced survival of lung tissue-resident memory CD8$^+$ T cells during infection with influenza virus due to selective expression of IFITM3. *Nat. Immunol.* 14:238–245. https://doi.org/10.1038/ni.2525

Wei, X., J.M. Decker, H. Liu, Z. Zhang, R.B. Arani, J.M. Kilby, M.S. Saag, X. Wu, G.M. Shaw, and J.C. Kappes. 2002. Emergence of resistant human immunodeficiency virus type 1 in patients receiving fusion inhibitor (T-20) monotherapy. *Antimicrob. Agents Chemother.* 46:1896–1905. https://doi.org/10.1128/AAC.46.6.1896-1905.2002

Williams, D.E., W.L. Wu, C.R. Grotefend, V. Radic, C. Chung, Y.H. Chung, M. Farzan, and I.C. Huang. 2014. IFITM3 polymorphism rs12252-C restricts influenza A viruses. *PLoS One.* 9:e110096. https://doi.org/10.1371/journal.pone.0110096

Wyrzucki, A., C. Dreyfus, I. Kohler, M. Steck, I.A. Wilson, and L. Hangartner. 2014. Alternative recognition of the conserved stem epitope in influenza A virus hemagglutinin by a VH3-30-encoded heterosubtypic antibody. *J. Virol.* 88:7083–7092. https://doi.org/10.1128/JVI.00178-14

Wyrzucki, A., M. Bianchi, I. Kohler, M. Steck, and L. Hangartner. 2015. Heterosubtypic antibodies to influenza A virus have limited activity against cell-bound virus but are not impaired by strain-specific serum antibodies. *J. Virol.* 89:3136–3144. https://doi.org/10.1128/JVI.03069-14

Yount, J.S., B. Moltedo, Y.Y. Yang, G. Charron, T.M. Moran, C.B. López, and H.C. Hang. 2010. Palmitoylome profiling reveals S-palmitoylation-dependent antiviral activity of IFITM3. *Nat. Chem. Biol.* 6:610–614. https://doi.org/10.1038/nchembio.405

Yount, J.S., R.A. Karssemeijer, and H.C. Hang. 2012. S-palmitoylation and ubiquitination differentially regulate interferon-induced transmembrane protein 3 (IFITM3)-mediated resistance to influenza virus. *J. Biol. Chem.* 287:19631–19641. https://doi.org/10.1074/jbc.M112.362095

Yu, J., M. Li, J. Wilkins, S. Ding, T.H. Swartz, A.M. Esposito, Y.M. Zheng, E.O. Freed, C. Liang, B.K. Chen, and S.L. Liu. 2015. IFITM Proteins Restrict HIV-1 Infection by Antagonizing the Envelope Glycoprotein. *Cell Rep.* 13:145–156. https://doi.org/10.1016/j.celrep.2015.08.055

Zhang, Y.H., Y. Zhao, N. Li, Y.C. Peng, E. Giannoulatou, R.H. Jin, H.P. Yan, H. Wu, J.H. Liu, N. Liu, et al. 2013. Interferon-induced transmembrane protein-3 genetic variant rs12252-C is associated with severe influenza in Chinese individuals. *Nat. Commun.* 4:1418. https://doi.org/10.1038/ncomms2433

Supplemental material

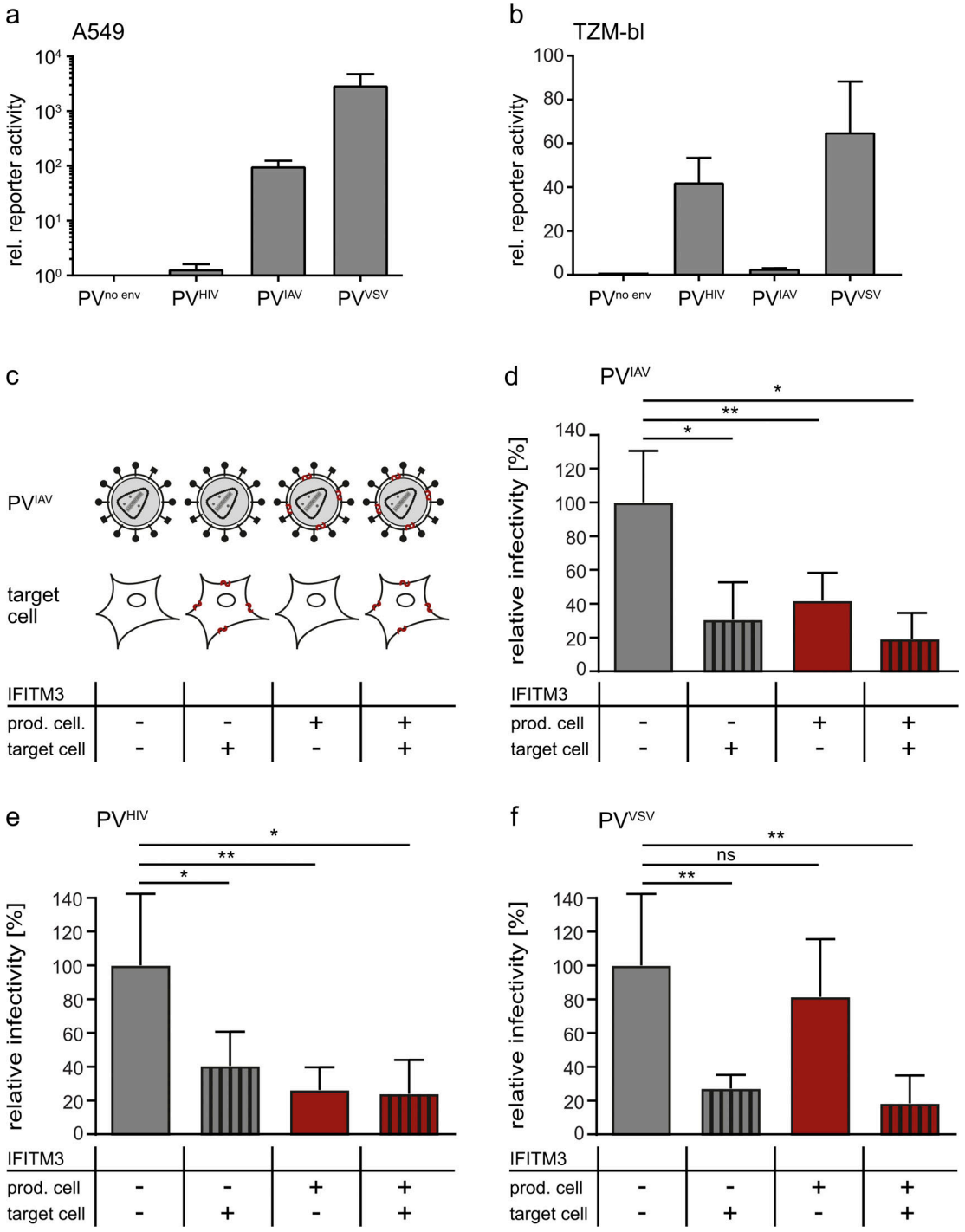

Figure S1. **IFITM3 reduces PV infectivity at the level of producer and target cell for IAV and HIV-1 but not for VSV in an HIV-1–based PV system. (a and b)** A549 cells (a) or TZM-bl cells (b) were infected for 48 h with the indicated PVs produced in the absence of IFITM3. Luciferase expression obtained after infection with $PV^{no\ env}$ was set to 1 and used to normalize luciferase values. Mean values from at least three independent replicates are shown with error bars representing SD. **(c)** Schematic depiction of PV^{IAV} produced in the absence or presence of IFITM3 and the cell lines, which were control transduced or transduced to stably express IFITM3. **(d)** A549 control cells or A549-IFITM3 cells were infected for 48 h with PV^{IAV} produced in the absence or presence IFITM3. Luciferase activity was measured and infectivity calculated by setting values obtained for A549 control cells infected with PV^{IAV} produced in the absence of IFITM3 to 100%. **(e)** TZM-bl control cells or TZM-bl-IFITM3 cells were infected for 48 h with PV^{HIV} produced in the absence or presence IFITM3. Luciferase activity was measured and infectivity calculated by setting values obtained for TZM-bl control cells infected with PV^{HIV} produced in the absence of IFITM3 to 100%. **(f)** TZM-bl control cells or TZM-bl-IFITM3 cells were infected for 48 h with PV^{VSV} produced in the absence or presence of IFITM3. Luciferase activity was measured and infectivity calculated by setting values obtained for TZM-bl control cells infected with PV^{VSV} produced in the absence of IFITM3 to 100%. **(d–f)** Mean values from three biological replicates, each performed in triplicates, are shown with error bars representing SD. Statistical significance was assessed by a paired two-tailed Student's *t* test (*, $P < 0.05$; **, $P < 0.01$), comparing infectivity in the different conditions with infectivity of PVs produced in the absence of IFITMs on IFITM3-negative cells.

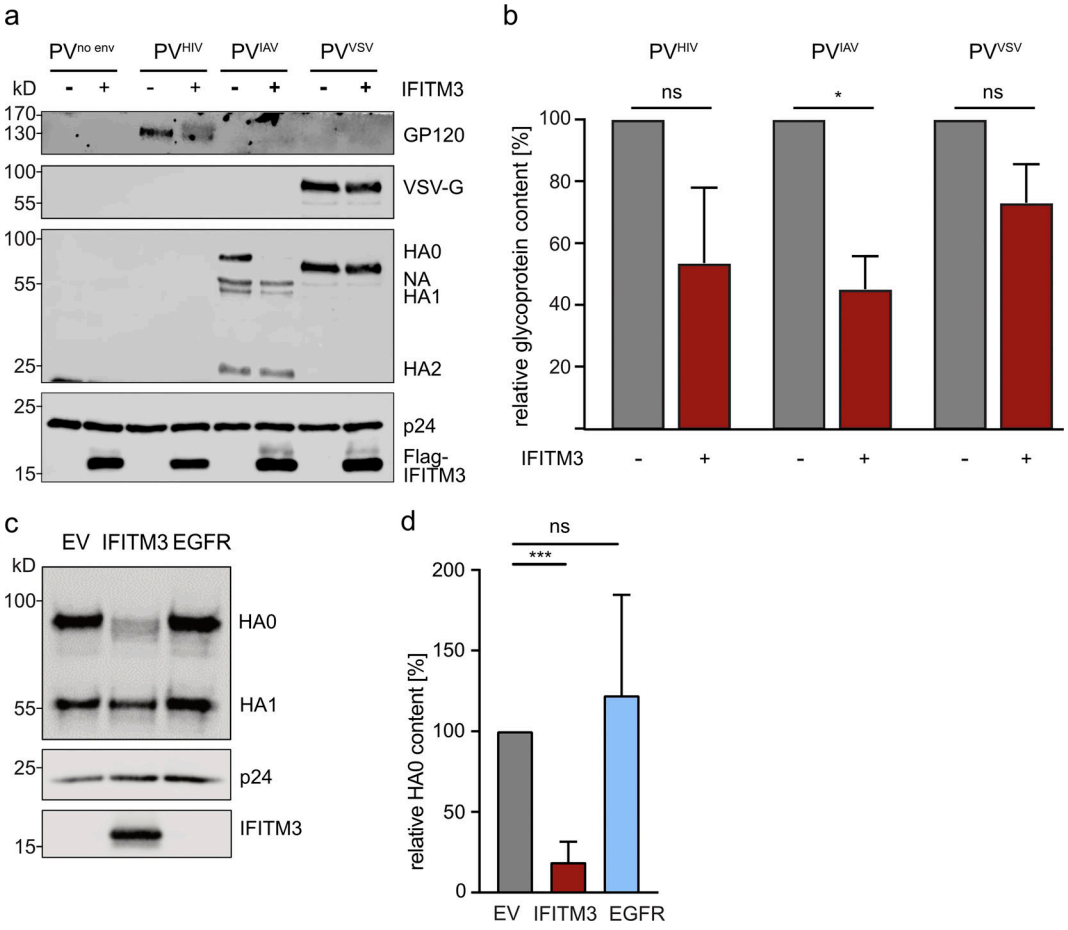

Figure S2. **PV^{HIV} and PV^{IAV} display decreased glycoprotein levels when produced in IFITM3-expressing cells but not in EGFR-expressing cells. (a and b)** The PV samples described in Fig. 1 were analyzed by Western blot using antibodies against p24, Flag, HIV-1 Env, VSV-G, and A/WSN/33 proteins. A representative blot (a), as well as the quantification of normalized GP120, HA, or VSV-G signal intensities from Western blots performed using three independent PV batches (b), are shown. Statistical significance was assessed by a paired two-tailed Student's *t* test. *, P < 0.05. The blots for p24 and Flag-IFITM3 are already shown in Fig. 1 b and are shown again here as input controls. **(c and d)** PVs PV^{IAV} were produced in the presence of IFITM3 or EGFR or a vector control (EV), purified by ultracentrifugation through a 20% sucrose cushion, and analyzed by Western blot. Membrane was stained with anti-IFITM3, anti-p24, and anti-HA antibodies. A representative blot is shown in panel c, and a quantification of HA0 content from three independent batches of PV^{IAV} is depicted in panel d. Error bars represent SD. Statistical significance was assessed by a paired two-tailed Student's *t* test. ***, P < 0.001.

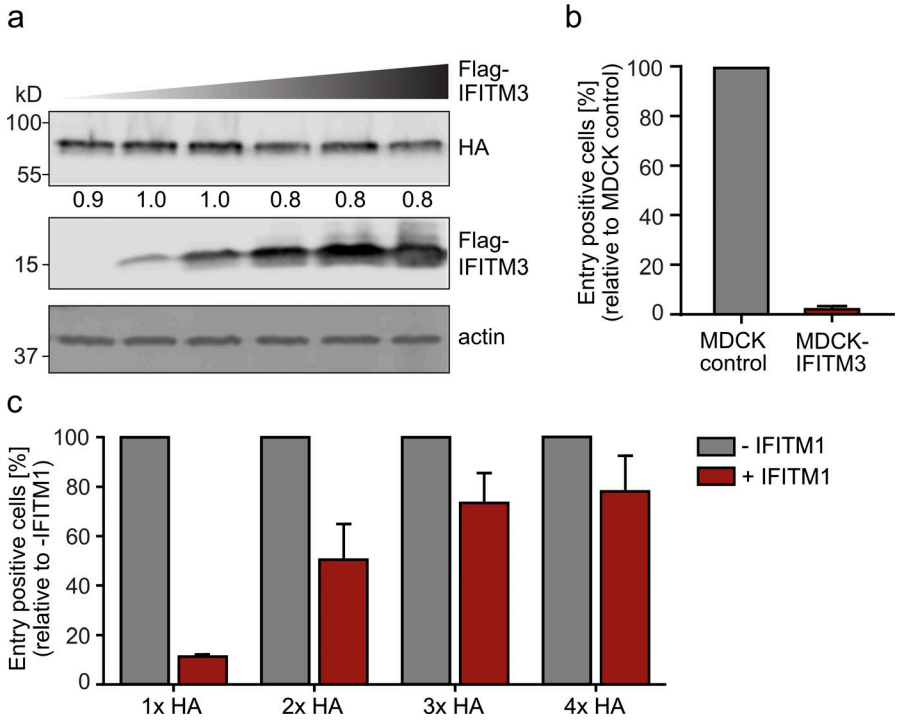

Figure S3. **IFITM3 expression does not lead to reduced cellular HA levels, and IFITM3 shares the ability to reduce IAV-VLP infectivity with IFITM1. (a)** HEK 293T cells were cotransfected with pCAGGS-HA and increasing amounts of pCAGGS-Flag-IFITM3. Whole-cell lysates were analyzed by Western blot and membrane was stained for HA, Flag, and actin. Expression levels of HA0 in relation to the strongest band are given below the blot. **(b)** MDCK control and MDCK-IFITM3 cells were infected with IAV-VLPs produced in the absence of IFITM3. Entry-positive cells relative to MDCK control cells are shown from three independent biological replicates with error bars representing SD. **(c)** IAV-VLPs containing increasing amounts of HA were produced in the absence or presence of IFITM1 and were used to infect MDCKII cells. For each condition, infectivity of IAV-VLPs produced in the absence of IFITM1 was set to 100%. Bars represent the mean of two biological replicates with the error bars representing SD.

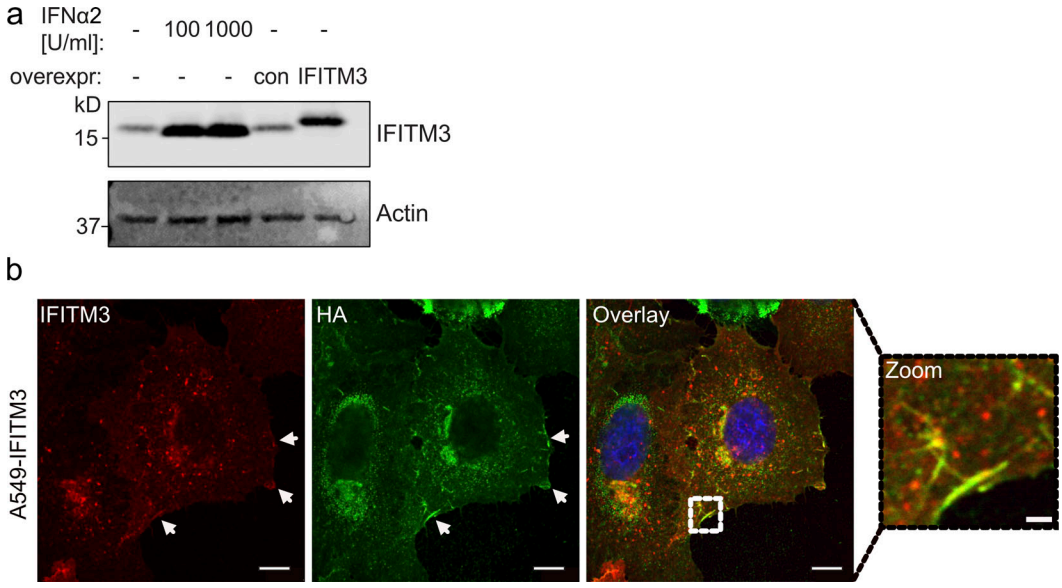

Figure S4. **IFITM3 is expressed to similar levels in A549-IFITM3 and IFN-treated A549 cells and colocalizes with HA during IAV infection. (a)** A549 cells were treated with 0, 100, or 1,000 U/ml IFN-α2 for 16 h before cells were lysed. In parallel, lysates of A549 control cells or A549-IFITM3 cells were prepared, and all lysates were tested for IFITM3 expression by Western blot. Actin staining was included as loading control. **(b)** A549-IFITM3 cells were infected with A/WSN/1933 (MOI 1) for 16 h. Cells were fixed and stained for DAPI (blue), HA (green), and IFITM3 (red). Samples were analyzed by confocal microscopy and a representative cell is shown with the indicated zoom area. Areas of colocalization at the plasma membrane are highlighted by arrows. Scale bars correspond to 25 µm or 1.5 µm for the higher magnification.

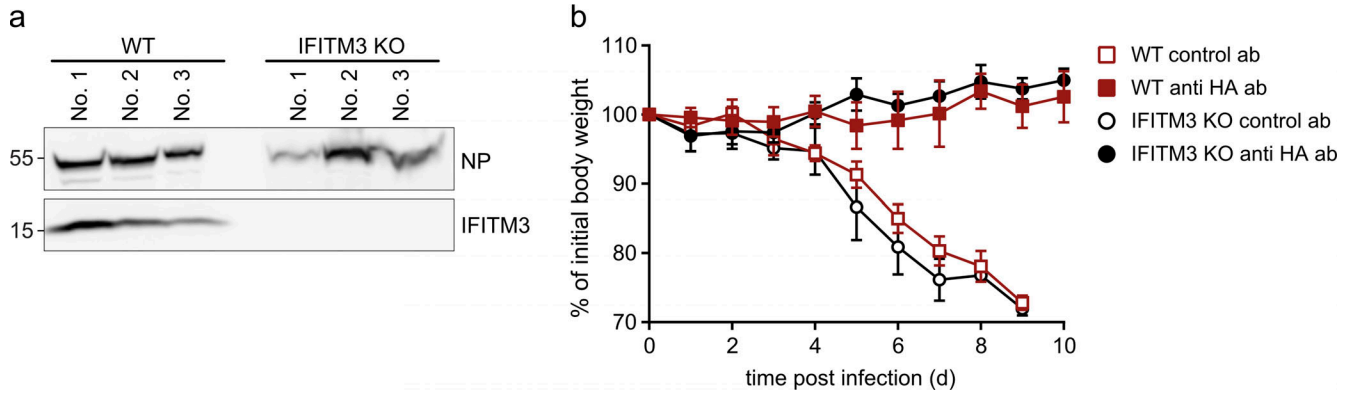

Figure S5. **A high dose of an HA head-specific antibody can protect WT and IFITM3 knockout mice from disease. (a)** Lungs from three IAV-infected WT and three IAV-infected IFITM3 knockout mice were harvested, homogenized, and analyzed by Western blot for IFITM3 and viral NP levels. **(b)** Morbidity upon lethal PR8 challenge (80 PFU) in IFITM3 knockout and WT mice 4 h after administration of a high dose of a PR8 HA head-specific antibody (2.5 mg/kg) or a control antibody. Error bars represent SD.